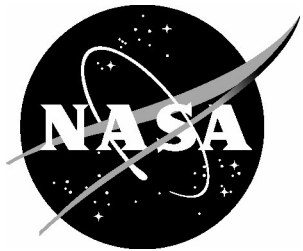


NASA/TP-2004-213247



Free-Stream Turbulence Intensity in the Langley 14- by 22-Foot Subsonic Tunnel

Dan H. Neuhart and Catherine B. McGinley
Langley Research Center, Hampton, Virginia

August 2004

The NASA STI Program Office . . . in Profile

Since its founding, NASA has been dedicated to the advancement of aeronautics and space science. The NASA Scientific and Technical Information (STI) Program Office plays a key part in helping NASA maintain this important role.

The NASA STI Program Office is operated by Langley Research Center, the lead center for NASA's scientific and technical information. The NASA STI Program Office provides access to the NASA STI Database, the largest collection of aeronautical and space science STI in the world. The Program Office is also NASA's institutional mechanism for disseminating the results of its research and development activities. These results are published by NASA in the NASA STI Report Series, which includes the following report types:

- **TECHNICAL PUBLICATION.** Reports of completed research or a major significant phase of research that present the results of NASA programs and include extensive data or theoretical analysis. Includes compilations of significant scientific and technical data and information deemed to be of continuing reference value. NASA counterpart of peer-reviewed formal professional papers, but having less stringent limitations on manuscript length and extent of graphic presentations.
- **TECHNICAL MEMORANDUM.** Scientific and technical findings that are preliminary or of specialized interest, e.g., quick release reports, working papers, and bibliographies that contain minimal annotation. Does not contain extensive analysis.
- **CONTRACTOR REPORT.** Scientific and technical findings by NASA-sponsored contractors and grantees.

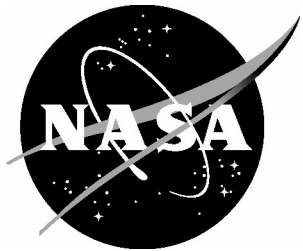
- **CONFERENCE PUBLICATION.** Collected papers from scientific and technical conferences, symposia, seminars, or other meetings sponsored or co-sponsored by NASA.
- **SPECIAL PUBLICATION.** Scientific, technical, or historical information from NASA programs, projects, and missions, often concerned with subjects having substantial public interest.
- **TECHNICAL TRANSLATION.** English-language translations of foreign scientific and technical material pertinent to NASA's mission.

Specialized services that complement the STI Program Office's diverse offerings include creating custom thesauri, building customized databases, organizing and publishing research results ... even providing videos.

For more information about the NASA STI Program Office, see the following:

- Access the NASA STI Program Home Page at <http://www.sti.nasa.gov>
- E-mail your question via the Internet to help@sti.nasa.gov
- Fax your question to the NASA STI Help Desk at (301) 621-0134
- Phone the NASA STI Help Desk at (301) 621-0390
- Write to:
NASA STI Help Desk
NASA Center for AeroSpace Information
7121 Standard Drive
Hanover, MD 21076-1320

NASA/TP-2004-213247



Free-Stream Turbulence Intensity in the Langley 14- by 22-Foot Subsonic Tunnel

Dan H. Neuhart and Catherine B. McGinley
Langley Research Center, Hampton, Virginia

National Aeronautics and
Space Administration

Langley Research Center
Hampton, Virginia 23681-2199

August 2004

The use of trademarks or names of manufacturers in the report is for accurate reporting and does not constitute an official endorsement, either expressed or implied, of such products or manufacturers by the National Aeronautics and Space Administration.

Available from:

NASA Center for AeroSpace Information (CASI)
7121 Standard Drive
Hanover, MD 21076-1320
(301) 621-0390

National Technical Information Service (NTIS)
5285 Port Royal Road
Springfield, VA 22161-2171
(703) 605-6000

Contents

Summary	1
Introduction	1
Nomenclature.....	2
Background	4
Experimental System Facility and Test Technique	5
Test Configuration	5
BLRS Suction Surface Replacement.....	5
Flow Quality Survey	6
Instrumentation	7
Pressure and Temperature.....	7
Hot-Wire Probes.....	7
Hot-Wire Setup and Calibration.....	8
Dynamic Data Acquisition and Analysis	9
Analysis of Results	10
BLRS Suction Surface Replacement Study.....	10
Old Suction Surface	12
New Suction Surface.....	13
Flow Quality Survey Test.....	14
General Features.....	14
Vertical Variation of TI	16
Streamwise Variation of TI.....	17
Concluding Remarks	18
Figures.....	19
Appendix.....	53
References.....	59

Summary

An investigation was conducted using hot-wire anemometry to determine the turbulence intensity levels in the test section of the Langley 14- by 22-Foot Subsonic Tunnel in the closed or “walls-down” configuration. This study was one component of the three-dimensional High-Lift Flow Physics experiment designed to provide code validation data. Turbulence intensities were measured during two stages of the study. In the first stage, the free-stream turbulence levels were measured before and after a change was made to the floor suction surface of the wind tunnel’s boundary layer removal system. The results indicated that the new suction surface at the entrance to the test section had little impact on the turbulence intensities. The second stage was an overall flow quality survey of the empty tunnel including measurements of the turbulence levels at several vertical and streamwise locations. Results indicated that the turbulence intensity is a function of tunnel dynamic pressure and the location in the test section. The general shape of the frequency spectrum is fairly consistent throughout the wind tunnel, changing mostly in amplitude (also slightly with frequency) with change in condition and location.

Introduction

The free-stream turbulence intensities (TIs) in the Langley 14- by 22-Foot Subsonic Tunnel were measured as part of the three-dimensional High-Lift Flow Physics (3-D HLFP) experiment. The 3-D HLFP experiment, funded under the Aerospace Systems Concept to Test (ASCoT) Project, was designed to investigate the complicated flow physics on a three-element, high-lift, semispan wing model and to provide data needed by computational fluid dynamicists to improve the prediction of these flows. In order to provide as complete a data set as possible, the 3-D HLFP experiment included measurements of the empty tunnel spatial distributions of flow angle, temperature, pressure, and TIs. Data collected on the model included boundary layer transition and separation locations. Additionally, off-body measurements were made of the velocity flow field. This report focuses on the free-stream turbulence data, which is of significant importance in the interpretation of the transition data and in subsequent attempts to computationally predict the transition locations.

The hot-wire measurements described in this report were obtained during two separate stages of the 3-D HLFP experiment. The first stage was an investigation into the effect of replacing the floor suction surface in the wind tunnel boundary layer removal system (BLRS). The second stage was a flow quality survey of the empty tunnel that included measurement of free-stream turbulence at several locations in the tunnel.

In the Langley 14- by 22-Foot Subsonic Tunnel, the floor boundary layer is removed by suction through a surface at the entrance to the test section. In preparing for the 3-D HLFP test, it was noticed that the suction surface was particularly rough, which would cause artificial thickening of the tunnel floor boundary layer. Because the 3-D HLFP model would be mounted on the floor, it was important to reduce the size of the floor boundary layer to minimize the flow interference. The new suction surface was designed to reduce the high surface roughness of the old surface. Turbulence measurements were made to determine if any change was made to the wind tunnel turbulence environment due to the installation of the new boundary layer removal suction surface.

After the BLRS issues were addressed, a flow quality survey was made of the empty test section with the new suction surface in place. These measurements were made to support future computations of the 3-D HLFP wing model’s flow field. Ideally, inflow/outflow measurements should include the influence of the model on the flow field; however, computationalists involved in this test deemed the empty tunnel measurements suitable. The measurements will also prove useful as a portion of the facility’s overall

calibration. Total and static pressure, temperature, flow angularity, and TI were measured in the wind tunnel's empty test section. Measurements were made at several locations in the test section and across the tunnel operating range of free-stream dynamic pressure. Only the results of the turbulence measurements are presented in this report.

Results of the measurements from the BLRS suction surface replacement study and the flow quality survey are provided as TIs at various tunnel free-stream dynamic pressures with floor boundary layer suction off and on. In addition, selected frequency spectra, in the form of power spectral density, are provided as needed to illustrate frequency-related phenomena of interest. The data are presented at several measurement stations, which vary in both longitudinal location and height in the test section. The effects of these location changes on TI are shown. An uncertainty analysis of the current data is given in the appendix.

Nomenclature

<i>A</i>	constant in equation (2)
AC	alternating current, fluctuating signal
A/D	analog-to-digital
ASCII	text data
ASCoT	Aerospace Systems Concept to Test
<i>B</i>	bias error (index) in measured or calculated quantity, or constant in equation (2)
BLRS	boundary layer removal system
BPF	blade passage frequency
<i>C</i>	constant in equation (2)
<i>D</i>	constant in equation (2)
DAS	data acquisition system
dB	decibel
DC	direct current, mean signal level
DMM	digital multimeter
<i>E, e</i>	electrical voltage, volts
ESP	electronically scanned pressure
<i>F</i>	constant in equation (2)

FS	full scale
fbw	full bandwidth
G_{nn}	noncoherent one-sided power spectral density, (ft/s) ² /Hz, or (ft/s) ² /(cycles/s)
G_{yy}	one-sided power spectral density, (ft/s) ² /Hz, or (ft/s) ² /(cycles/s)
i	electrical current (fig. 3(b))
L	constant in equation (1)
M	Mach number, or constant in equation (1)
m	temperature loading factor, empirical factor in equation (3)
n	exponent in equation (1)
P	precision error (index) in measured or calculated quantity
PS	pitot-static
PSD	power spectral density
Q	wind tunnel dynamic pressure, lb/ft ²
R	resistance, ohms
R_{ext}	variable resistor
rms	root-mean-square
rss	root-sum-square
SN	single-normal
T	temperature, F or K
TI	turbulence intensity
U	mean velocity, ft/s, or uncertainty in calculated quantity or result
u'_i	instantaneous fluctuating velocity, ft/s
u_{rms}	root-mean-square fluctuating velocity, ft/s
X	longitudinal location in test section, ft
x_i	measured quantity

Y	lateral location in test section, ft
Z	vertical location in test section, ft or in.
γ_{xy}	coherence function
Δ	uncertainty in measured quantity
∂	partial derivative
τ	hot-wire overheat ratio, $(T_w - T_a)/T_w$
Ω	ohms
3-D HLFP	three-dimensional High-Lift Flow Physics

Subscripts:

1	ambient condition at time of data acquisition
a	ambient or conditions at wire overheat setup
corr	corrected quantity
N	total number of data points
nom	nominal or typical conditions
r	result
s	static
t	total
w	wire

Background

One of the most challenging aspects of computing high-lift configurations is the prediction of transition. The location of the transition region on a surface can be affected by many factors, one of them being wind tunnel free-stream turbulence. These free-stream disturbances can enter a model's boundary layer and excite its various instability modes (ref. 1). Excitation at discrete frequencies can lead to the amplification of these modes, resulting in boundary layer instability and, eventually, turbulent flow in the boundary layer. If the boundary layer excitation frequencies coincide with those of the free-stream tunnel disturbances, and the amplitudes are large enough, then the free-stream turbulence may prompt early transition in the model boundary layer. Some general guidelines have been proposed for low-turbulence wind tunnels in terms of both TI and measurement bandwidth (refs. 2 and 3), ranging from 0.05 to 0.07 percent and 0.1 to 10 kHz, respectively.

The measurements of TIs are usually conducted using hot-wire anemometry. Hot-wire anemometry has its origin in the 19th century; however, practical application moved toward maturity in the first half of the 20th century. It was still primarily an art until the last half of the 20th century, when it became established as a “standard experimental method” (ref. 4). By 1980, over 1600 references had been identified, and although the rate of publication on the technique had declined, this method still remains the standard for measuring free-stream TI and time series data in fluid flow. The primary reference book on hot-wire anemometry describing in detail the fundamental principles in detail was written by Perry (ref. 5). A text on the practical use of the technique by Bruun (ref. 6) provides an important reference for the use of hot-wire/hot-film methods, as well as an extensive bibliography.

The most common hot-wire anemometer system in use today is the constant temperature system. In this system, the temperature of the wire is kept constant by a feedback circuit in the anemometer. When the wire is placed in the flow, it is cooled by convective heat transfer to the air. This cooling of the wire reduces its temperature and, hence, the electrical resistance. The feedback circuit, sensing reduced voltage, increases voltage output to the wire circuit, which in turn increases the current to keep the wire at a constant resistance and therefore a constant temperature. The variations in current as the velocity across the wire fluctuates are manifested as variations in voltage. Through the convective heat transfer relationship, these voltage signal variations are converted to fluctuations in velocity from which the TI is computed.

Experimental System Facility and Test Technique

The Langley 14- by 22-Foot Subsonic Tunnel is a closed-circuit, atmospheric-pressure wind tunnel capable of operating in an open, partially closed, or closed test section mode. A schematic of the facility is shown in figure 1. Raising and lowering of the north and south walls (see fig. 2(a)) and ceiling creates the various modes of tunnel geometry. The floor of the test section is formed by two model “carts” that are moved to and from the test section front and back bays. The carts are raised and lowered on hydraulic lifts and transported along the floor under the test section on air pads. Once in place, the tunnel floor is fixed during testing. Measurements for this test were made in the closed test section mode. In this mode, the test section measures 14.5 ft high and 21.75 ft wide, and the maximum free-stream velocity is 338 ft/s. The tunnel contraction ratio is 9 to 1. Further details about the tunnel can be found in reference 7.

Test Configuration

For the BLRS suction surface replacement study and the flow quality survey, multiple hot-wire probes were placed in the wind tunnel in different configurations. In order to use data reduction techniques to isolate the turbulence portion of the hot-wire signal, data from at least two hot-wire probes were recorded at all times. The hot-wire probes that were used only to remove extraneous signals from the primary hot-wire signals are referred to as the “noise cancellation wires.” Due to expected wire breakage, provisions were made to mount extra hot-wire probes when possible.

BLRS Suction Surface Replacement

For the suction surface study, as shown in figure 2(a), three single-normal hot-wire probes were mounted in the wind tunnel. A single hot-wire probe was placed at the end of a boundary layer rake attached to the tunnel’s north sidewall. The rake was located 94 in. downstream of the test section entrance and 88.25 in. above the tunnel floor. The hot-wire probe, which was placed at the end of the rake, extended out approximately 17.5 in. from the sidewall. The other two hot-wire probes were placed on a stand mounted on the floor at the end of the test section. The stand with two hot-wire probes also held a

total temperature probe and a pitot-static (PS) probe. It was located 35 in. downstream of the back edge of the aft model cart. This placed these probes slightly into the first diffuser of the tunnel and about two test section widths downstream of the wall-mounted probe. These two measurement locations can be seen in figure 2(a). The coordinates for the probes are listed in table 1 and the coordinate system is labeled in figure 2(a). For the BLRS study, the stand probes provided the primary hot-wire data and the north wall probe acted as the noise cancellation wire.

Table 1. Hot-Wire Probe Location for BLRS Grate Replacement Study

Probe	X, ft	Y, ft	Z, ft
North wall	7.83	-9.42	7.35
Stand #1	53.15	-5.75	4.88
Stand #2	53.15	-5.75	4.46

Flow Quality Survey

For the flow survey test, four hot-wire probes were placed in the test section. Two wires resided on a test section survey-rake and two wires were mounted at different locations, depending on the location of the test section survey-rake. The test section survey-rake spanned the test section's width (fig. 2(b)). The rake contained 26 probes of various types (seven-hole, PS, thermocouple, hot-wire) and was capable of being located at five vertical stations and four longitudinal stations in the test section. The rake was attached to the tunnel sidewalls on each end and stabilized with eight cables, four above and four below, attached to the rake with cable brackets. Due to time constraints, limited vertical locations were attained at longitudinal stations at the front of the test section, in the middle of the front bay, and in the middle of the back bay.

To measure the free-stream turbulence, two hot-wire probes resided on the rake and were flanked by PS probes and temperature probes. The wires were mounted, as shown in figure 2(b), 18 and 30 in. laterally from the test section center. Six inches outside of each hot-wire probe were mounted PS probes, and outside of each PS probe was a total temperature probe.

When the full-span rake was in the test section's front bay, over the front model cart, the remaining two hot-wire probes were located on the stand in the test section's aft part—the same location as for the suction surface study. When the rake was in the back bay, the stand was removed and the two hot-wire probes were located at the end of two wall boundary layer rakes, at the same longitudinal and vertical locations on opposing walls in the test section's front bay. Figure 2(c) schematically shows the various longitudinal locations of the full-span rake with the six probes in their approximate locations on the rake (other probes not shown). The wall boundary layer rakes are shown on the walls. The stand is shown in the back of the test section. Locations for the various configurations are listed in table 2. For the flow survey study, the test section survey-rake wires served as the primary hot-wire probes with the stand and wall-mounted wires acting as the noise cancellation wires.

Table 2. Hot-Wire Probe Locations for Flow Quality Survey Test

Test section survey-rake		Noise cancellation wires		
X, ft	Z, ft (in.)	X, ft	Y, ft	Z, ft
7.87	10.25 (123)	53.15	-5.75	4.88/4.46
7.87	7.25 (87)	53.15	-5.75	4.88/4.46
7.87	4.25 (51)	53.15	-5.75	4.88/4.46
17.75	7.25 (87)	53.15	-5.75	4.88/4.46
17.75	4.25 (51)	53.15	-5.75	4.88/4.46
40.00	10.25 (123)	7.83	± 9.42	7.35

Instrumentation

The instrumentation system is illustrated schematically in figure 3(a). Components for measuring voltage from the hot-wire probe are shown in the top part of the figure, and those associated with the measurement of local velocity, for hot-wire probe calibration purposes, are shown in the bottom.

Pressure and Temperature

Starting at the bottom of figure 3(a), pressure and temperature (thermocouples) probes were used to determine local velocity in the vicinity of the hot-wire probes. For the wall-mounted boundary layer rake, the total pressure tube farthest from the wall and a static orifice, flush with the wall near the base of the rake, were used to sense pressures for the rake-mounted hot-wire probe. PS probes sensed local total and static pressures for probes on the stand in the back of the test section and for test section survey-rake mounted probes.

The pressure transducer used for the probe stand and for the wall-mounted rake during the BLRS suction surface replacement study was a high-precision, capacitive potentiometer containing a metal diaphragm as the movable sensing element. The total pressure was sensed as an absolute pressure, and the static pressure was determined from the sensed differential pressure between total and static pressures. Signals from this sensor were sent to the tunnel data acquisition system (DAS) via a “send” task over an ethernet line.

During the flow quality survey test, for the test section survey rake and for the wall-mounted rake, pressure sensing was performed using an electronically scanned pressure (ESP) transducer. For this test, 48-port modules were used. These modules each contain an array of silicon piezoresistive pressure sensors, one per port, that measure differential pressure. The sensor outputs are electronically multiplexed and sent to an analog-to-digital (A/D) converter in the ESP transducer instrumentation package. The digital signal is then sent to the DAS via ESP transducer instrumentation.

Hot-Wire Probes

At the top of figure 3(a), the hot-wire probe is a single-normal (SN) probe. This probe suspends a platinum-plated tungsten wire 5 μm in diameter, which is plated with copper and etched in the middle, across two tapered prongs with the wire perpendicular to oncoming flow. One velocity component was measured based on analysis of the electrical signal. Placed normal to oncoming free-stream flow, the probe measured the total instantaneous free-stream velocity.

The anemometer unit sends the voltage signal (mean plus fluctuating signal) to an output that is split before filtering. The electronic arrangement of the anemometer bridge circuit (fig. 3(b)) was in the 1 to 1 configuration with an external resistance arm containing a variable resistor, R_{ext} . This resistor allows the user to adjust the hot-wire overheat ratio, τ , to the desired level, a level high enough to make the wires sensitive primarily to velocity fluctuations (typically, $\tau = 0.9$).

In figure 3(a), the filter unit takes each anemometer output and filters it separately as alternating current (AC) (fluctuating) and direct current (DC) (mean) voltage signals. The AC signal is band pass filtered between 1 and 10 kHz. The DC signal is low pass filtered at 1 Hz. The band pass filtering is accomplished with a high pass filter followed by a low pass filter. The filters have an 80-dB/octave rolloff and a ± 0.05 -dB accuracy in the pass band. They are elliptic-type, 6-pole/6-zero filters with a 0.1- to 10 230-Hz high pass range and a 1- to 25 575-Hz low pass range. All channels were DC coupled with differential input. No pre- or postgains were applied to any channels.

The digitizer is a computer-controlled, 16-channel unit. Each channel had a 16-bit A/D converter. The digitizer is capable of sampling up to 51.2 kilosamples/s with input ranges from 100 mV to 10 V. The crosschannel phase match at 20 kHz is $\pm 2.5^\circ$. The digitized signals were sent to the data acquisition computer via a high-speed interface.

All instrumentation was powered from a circuit having an isolated electrical ground system to minimize electronic noise.

Hot-Wire Setup and Calibration

After installing the wires in their holders, overheat ratios were set on each wire using the external variable resistor in each anemometer circuit. Once the overheat ratios were set, wires were “tuned” at the highest test speed. A square-wave voltage signal was injected into the bridge, which was then tuned to optimize the system frequency response. In general, the bandwidth obtained at over 300 ft/s was at least 60 kHz.

Hot-wire probes require calibration to provide a relationship between the measured voltage and velocity at the probe. All the hot-wire probes were calibrated against a local measurement of the velocity. The calibration data are taken over a range of mean velocities exceeding the range to be tested. An adequate number of velocity set points (e.g., 15 to 20) must be chosen to yield a good curve fit of voltage versus velocity data. For the BLRS suction surface replacement study, calibration data were taken before time series data were acquired. In the flow quality survey test, however, time constraints limited the ability to run separate calibration runs; therefore, actual data runs were used for the calibration data as well. Fortunately, 15 to 17 velocity set points were acquired for each run. A decimated subset (providing independent samples) of data points for each mean velocity was used for the calibration data. In general, about 16 000 points were used for the calculation of each mean voltage.

The two most popular methods of relating hot-wire voltage to velocity are the power law and the polynomial curve fit. The power law method derives from the heat transfer relationship. It is a linear relationship between the mean voltage squared versus the mean velocity raised to some power,

$$E^2 = L + MU^n \quad (1)$$

Another standard method is a fourth-order polynomial curve fit of the voltage versus velocity data,

$$U = A + BE + CE^2 + DE^3 + FE^4 \quad (2)$$

Both methods provide similar accuracies and are entirely adequate (ref. 6). The polynomial fit was used for reducing the calibration data in this report.

Calibration of the hot-wire probe is sensitive to changes in total temperature. After the voltage signals were acquired, a temperature correction was made using an equation provided by the anemometer manufacturer. The equation for the corrected voltage is

$$E_{\text{corr}} = \left\{ \left[(T_w - T_a) / (T_w - T_1) \right]^{0.5(1 \pm m)} \right\} E_1 \quad (3)$$

where the temperature loading factor, m , was added or subtracted depending on whether the temperatures were increasing or decreasing, respectively (ref. 8). The correction is a function of the wire temperature, T_w , the reference temperature at setup (when overheat ratio was set), T_a , and the ambient temperature when the data point was acquired, T_1 . The corrections are specified to reduce the error due to temperature changes from ± 2 percent/ $^{\circ}\text{C}$ to ± 0.05 percent/ $^{\circ}\text{C}$. An example of a corrected calibration curve is shown in figure 4.

Dynamic Data Acquisition and Analysis

For the top tunnel speed of about 338 ft/s, the upper limit of desired frequency bandwidth of 10 kHz was found to be adequate. The lower bandwidth was set to 1 Hz. Some authors have suggested a lower limit of 0.1 Hz (ref. 9) for low speed tunnels because fluctuations below 1 Hz could make a significant difference in the overall TI value. A compromise was chosen, however, based on recommended standards of flow quality for laminar flow testing from reference 2. Because fluctuations at 1 Hz and below have an as-yet undefined effect on transition, we chose a lower limit of 1 Hz.

The digitizer sample rate was 25.6 kHz, 2.56 times the upper limit of the desired data bandwidth of 10 kHz. All channels were recorded simultaneously and the data were recorded continuously for 64 s, resulting in a data record of 1 638 400 points. Using 100 averages to compute the power spectrum resulted in a frequency resolution of 1.5625 Hz. All spectra were computed using a Hanning window.

Analysis of the random data taken in this experiment used methods that assume stationary data, meaning that the statistical quantities calculated are independent of time. Stationarity of the data was verified by examining the steadiness over time of the mean and mean square values of segments of the total time record. In addition, ensemble averages and their mean square values were verified for steadiness. Because these averages also equaled the time averages (ergodic), they could be replaced by time averages of single records, which could therefore be assumed to represent a sample from a stationary, random process (ref. 10).

Various inputs contribute to the hot-wire signal. While the vorticity is usually the strongest component, the signal is often contaminated by other influences, such as sound waves, temperature spots, and electronic noise. Acoustic disturbances can come from many sources, such as the fan, the motor, the turning vanes, the boundary layer, and the BLRS. Although these disturbances could contribute to premature model boundary layer transition under some circumstances, the subject of this investigation

was strictly a measurement of turbulence in the test section. Electrical noise can be introduced at any frequency, and, in particular, at the 60-Hz line frequency and its harmonics.

To isolate the vorticity signal, a technique was used that is based on the correlation of signals between two probes spaced some distance apart. Saric, Takagi, and Mousseux (ref. 9) discussed the concept of signals correlated over short distances, that is, the total signal (vortical plus acoustic) versus those correlated over long distances, or from acoustic disturbances alone. The size of the largest fluctuation due to turbulence in the test section would be, at most, the largest test section cross-sectional dimension. Spacing two probes at a distance larger than this would ensure that the *turbulent* fluctuations measured at these two locations would be uncorrelated (ref. 11). Because certain acoustic disturbances correlate over long distances, there should be a correlation of some acoustic signals between the two separated probes. (Not all acoustic signals will be correlated between the probes.) The difference, in the frequency domain, between the total signal and the signal correlated between the separated probes represents a better estimate of the vortical fluctuations (turbulence), which is the desired signal. Additionally, some electronic noise (specifically 60 cycle noise) may be common to both signals and would be reduced to some extent. For the sake of brevity, the process of removing correlated components of the sound and electronic noise from the total signal will simply be referred to as “noise removal.”

The noise-removal technique used in this investigation involved the use of the coherence function as described in reference 10. The coherence function is a measure of the power in one signal linearly related to the power in another signal. It is a function of frequency and, therefore, would vary across the bandwidth of the measurement. The coherence between the measurement probe and the noise-removal probe represents the portion of the measurement signal that was linearly related to the signal from the noise-removal probe (i.e., due primarily to correlated acoustic and electronic noise disturbances). To obtain the signal portion from the measurement probe not accounted for by the signal from the noise-removal probe (i.e., the vortical or turbulence contribution), the measured spectrum multiplied by the coherence is subtracted from the measured spectrum, yielding the noncoherent spectrum. The equation illustrating the process is

$$G_{nn} = \left(1 - \gamma_{xy}^2\right) G_{yy} \quad (4)$$

G_{nn} , then, represents the spectrum with the correlated noise removed.

Analysis of Results

BLRS Suction Surface Replacement Study

The suction surface replacement study was conducted to discover any significant effects manifested in the wind tunnel turbulence environment due to the installation of a new suction surface in the BLRS. Both the old and new suction surfaces are shown schematically in figure 5. Located at the tunnel entrance on the floor, the old suction surface had parallel, longitudinal slots 0.625 in. wide and 7.5 in. long that were spaced laterally by 0.875 in. The suction surface spanned the width of the tunnel and was about 63 in. long in the tunnel longitudinal direction, starting 1 ft from the test section entrance. The new suction surface is a porous surface with a staggered hole pattern of 0.125-in-diameter holes on 0.1875-in. centers. The surface extends 14 in. in the tunnel longitudinal direction and spans the tunnel except for about 10 in. on each end. The porous surface starts 36 in. downstream of the test section entrance.

The main reason for replacing the original suction surface was that it had a high degree of surface roughness that likely caused an artificial thickening of the tunnel floor boundary layer. Previous measurements of the boundary layer height on the floor, taken at the center of the first cart ($X = 17.75$ ft) at $Q = 60$ psf, indicated that the boundary layer height was approximately 11 in. without suction and 3 in. with suction (ref. 7). For the new suction surface, boundary layer measurements were only available upstream at $X = 7.87$ ft. At this location, the boundary layer height was approximately 4.2 in. without suction and 1.0 in. with suction. Using these measurements and calculations from reference 12, we estimate that the boundary layer size at the $X = 17.75$ ft location would be approximately 7 in. without suction and 2.5 in. with suction for the new suction surface. These reductions in the boundary layer height, of approximately 4 in. without suction and 0.5 in. with suction, should result in decreased flow interference with the semispan model mounted at this location.

To detect any difference in the turbulence environment due to the suction surface replacement, hot-wire probes were mounted on the tunnel wall and a stand at the rear of the test section. The hot-wire probe mounted on the tunnel sidewall boundary layer rake was to be the primary measurement of turbulence in the test section for this study. However, examination of the time record of the signal indicated a large number of disturbances in the signal that were not characteristic of free-stream turbulence (fig. 6(a)). Closer examination indicated that the nature of the disturbance was likely a fluid mechanic interaction, as seen in figure 6(b). The number of intermittent disturbances increased as the tunnel dynamic pressure (Q) increased. Because the hot-wire probe was over 17 in. from the wall, and the wall boundary layer was known to be only about 4 to 5 in. thick, it was more likely that the source of disturbances in the time record originated upstream.

Examination of the honeycomb upstream of the four turbulence-reduction screens, just ahead of the tunnel contraction section, revealed some seams between sections of honeycomb. However, accounting for the tunnel contraction into the test section, the effect of the seam in the honeycomb would likely be too far away from the wall to have an impact. Another candidate for the source of disturbance was the tunnel static pressure probe mounted on the tunnel sidewall, at the end of the contraction, about 20 ft upstream of and 8 in. below the hot-wire probe. The static pressure probe is 14 in. long and 0.25 in. in diameter. Because the probe is over 900 diameters upstream of the hot-wire sensor, it is possible that the unsteady wake generated by the pressure probe had spread/moved enough vertically (due to tunnel flow angularity) to provide an intermittent interaction with the hot-wire probe. A third source possibility is flow from a gap upstream of the hot-wire probe where the contraction section connects to the test section sidewall.

The signals acquired from the hot-wire probes on the stand in the aft part of the test section did not show disturbances seen on the sidewall-mounted probe. They were therefore considered more appropriate for use as signal probes, and thus the wall-mounted probe was used as the noise-removal probe. The power spectral density (PSD) of signals from the hot-wire probe on the wall versus the one on the stand, at $Q = 59$ psf, is shown in figure 7. Intermittent disturbances on the wall probe appeared to impose a detrimental contamination effect on the signal (i.e., an increase in TI of 12 percent).

Examination of the hot-wire signal in the frequency domain revealed a number of very sharp spikes in all of the spectra, starting at 180 Hz. Further inspection of these spikes indicated that they were odd multiples of 60 Hz, the AC line voltage in the facility. Discussion with the facility electricians verified that this is a common facility characteristic. These peaks can be confirmed as electronic in nature by looking at figure 8, which shows a comparison of the spectrum at $Q = 59$ psf to a spectrum from data taken when the tunnel was not running, referred to as a “no flow” spectrum. In figure 8, the odd

harmonics of 60 Hz are still evident in the no flow spectrum as well as a peak representing the fundamental frequency at 60 Hz. If noise-removal techniques were applied to the data, one might inquire as to why the electronic noise spikes were still evident in the final PSDs. Due to the discrete nature of digital data acquisition, complete removal of noise from two separate channels is not possible. However, it was verified that the largest peaks were reduced by factors of 3 to 5. The remaining sharp spikes did not contribute significantly to the integrated root-mean-square (rms) velocities. For selected cases, the remaining noise spikes were removed out to frequencies as far as could be visually detected (eleventh harmonic), and the value of the TI was reduced by only 0.1 percent of the unaltered value. This change in value indicates that the electronic noise spikes, which remained in the spectra after application of the noise removal techniques, did not significantly contribute to the calculated TIs.

The no flow voltage spectrum (fig. 8) also gives an indication of the noise floor of the instrumentation. The increasing energy below 10 Hz is due to small residual airflow in the test section with the tunnel fan off, even though doors at each end of the test section were closed. It can be seen that the spectrum from the flow signal almost merges with the no flow spectrum at about 2000 to 3000 Hz. At higher frequencies, no flow spectral power is almost equal to signal power. For the flow signal shown in figure 8, contributions to TI from the frequency band 1 to 3000 Hz accounted for 82 percent of the total value. But because the noise floor of the system will change with the anemometer's operating point, and the point at which the signal level will disappear into the noise floor will change with tunnel conditions, the noise floor was not subtracted from the hot-wire signal. Thus the entire signal, from 1 to 10 kHz, was used to compute TI. This provides a consistent bandwidth for reporting tunnel turbulence conditions.

Old Suction Surface

Data were acquired over a range of tunnel free-stream dynamic pressure, Q , from 15 to 125 psf with the BLRS off and on. PSD data with the BLRS off are shown in figure 9(a) for five tunnel Q values. As tunnel Q increases, the level of the PSD increases, implying that the integrated rms velocity fluctuation will be higher at higher Q values. The normalized TI may or may not be higher, however, because the normalizing tunnel velocity will also increase with tunnel Q . As speed increases, the spectra "fill out" at higher frequencies, an effect most likely due to the increase in Reynolds number. Spectral peaks at frequencies of 20 and 27 Hz increase in amplitude with Q but stay at fixed frequencies. They may be related to vibration in the probe stand, probe holder, or probe. No accelerometers were attached to the stand to verify this. Michel and Froebel (ref. 13) noticed similar effects in spectra due to probe holders, for example. In the region between 70 and 300 Hz in figure 9(a), there is a group of peaks that appears and increases in amplitude as Q increases. In addition, these peaks appear to increase in frequency, as a group, as Q increases. The peaks could be related to nonuniform vortex stretching, across the frequency spectrum, in the tunnel contraction section. Reshotko, Saric, and Nagib (ref. 3) point out that high tunnel contraction ratios, 9 to 1 or greater, may exhibit a phenomenon related to vortex stretching that could cause a rise in the spectral amplitude in selected frequency ranges.

The effect of energizing the BLRS is shown in figure 9(b). The most noticeable change is that the low-frequency content of the spectra has been reduced at each value of Q . Using the methods of reference 12, we estimate that by the time the floor boundary layer reached the end of the test section, with the BLRS off, it may be 15 in. in height (and only half that with the BLRS on). Such a large boundary layer may separate in the diffuser section and be the source of the low frequency signal seen in the BLRS off data. The same spikes seen between 70 and 300 Hz in the BLRS off data are also seen in figure 9(b) for the BLRS on, especially for $Q = 60$ psf and above. Additionally, two sets of peaks occur at frequencies of 20 and 27 Hz whose frequencies do not change with Q and are therefore likely to be related to structural

vibration. They are slightly visible in figure 9(a), but the higher overall spectral levels mask their appearances. Figure 9(c) highlights the difference in the spectra for $Q = 33$ psf and $Q = 125$ psf for the BLRS off and on. As stated previously, the main difference between the spectra is a significant decrease in the low-frequency component of the spectra when the BLRS is on. At higher frequencies, however, it is interesting to note that the data show an increase in intensity with the BLRS on as compared with the BLRS off.

The resulting change in TIs is shown in figure 10. Clearly, for this configuration, the BLRS had an overall attenuating effect on TI across the range of Q . As evidenced by the spectral plots, the reduction is due to a decrease in energy in the low-frequency end of the spectra, which clearly offsets the small increase at the higher frequencies. The overall reduction in TI is relatively constant and shows that the BLRS suction reduced TI for all Q values by an average of 12.7 percent. The TI values remain fairly constant with Q for either the BLRS on or off. Where multiple symbols exist, repeat data were taken, and good repeatability is indicated. The TI values showed repeatability within about 2.5 percent.

New Suction Surface

After the new suction surface was installed, data were acquired over the same range of conditions as for the old suction surface and the hot-wire probes were configured in the same manner. Examination of frequency content of signals showed the same odd multiples of the 60-Hz line frequency as before, although at a lower amplitude. PSD data for the new BLRS suction surface, with the BLRS off, are shown in figure 11(a). As would be expected, the levels increase with increases in Q . There are new features in the spectra at frequencies above 1000 Hz in figure 11(a). At Q values of 59 psf and above, distinct peaks appear and increase in amplitude, while remaining at fixed frequencies, as Q increases. The five approximate frequencies at which these values occur are: 1250, 1600, 3500, 4750, and 7500 Hz. In addition, there was an isolated peak at about 1950 Hz for $Q = 87$ psf that had no corresponding peaks at other Q values. Acoustic microphone data taken for this BLRS grid showed peaks that change in frequency as Q changes, but at none of the above frequencies. The spectra from the sidewall-mounted probe were checked for presence of the high-frequency peaks. No similar peaks existed at high frequencies for the wall-mounted probe at the same tunnel conditions. Unfortunately, the second stand wire broke during these runs, so no comparison could be made at the same X location. While it is possible that these peaks were related to the hot-wire element, this wire was used to obtain data at an upstream location at the same Q values, and that data did not show the same spikes. That these spikes do not change with Q means they are not hydrodynamically generated and are of such low level that they do not significantly contribute to TI.

The effect of energizing the BLRS is shown in figure 11(b). In contrast to the old suction surface, there is no dramatic reduction in the low-frequency component of the spectra due to the BLRS. The peaks at 20 and 27 Hz and the spikes between 70 and 300 Hz, as well as those above 1000 Hz, show no appreciable change due to the BLRS being switched on. In figure 11(c), a comparison is made of the spectra for $Q = 33$ psf and Q at about 120 psf for the BLRS off and on. There are two noticeable differences at $Q = 33$ psf. The first is a spike at 50 Hz for the BLRS off that is not present when the BLRS is on. The second spike, at about 100 Hz and seen at higher Q s, is now more pronounced when the BLRS is on than when off. In general, at frequencies below approximately 100 Hz, for $Q = 33$ psf, the energy content is at first slightly higher and then lower for the BLRS on with increasing frequency. For the higher Q , at low frequencies, the energy level is higher with the BLRS on. At higher frequencies, the spectra are effectively the same for the BLRS on or off for each Q . The resultant effect of energizing the BLRS on TI values is shown in figure 12. In this case, there is not a consistent difference apparent between the BLRS

on and off conditions; however, except for the TI value at the lowest Q , the effect of increasing Q is an increase in TI.

TI values for both the new and old BLRS suction surfaces are shown in figure 13 for the BLRS off. Clearly, in terms of TI, the new BLRS suction surface had no detrimental effect. In fact, at low Q values, the TI values were lower for the new suction surface and significantly lower at a Q of about 33 psf. PSDs for the old and new suction surfaces at Q values of about 33 and 120 psf are shown in figures 14(a) and (b), respectively. In figure 14(a), where $Q = 33$ psf, the spectrum for the new suction surface is significantly reduced for frequencies less than 50 Hz. At high Q , in figure 14(b), initially the spectrum for the new surface is higher than the old until approximately 7 Hz. Between 7 and 70 Hz, the new surface spectrum is lower than the old. There are similar peaks in the spectra between 70 and 300 Hz with some slight shifting in frequency. New, high-frequency peaks are seen to emerge with the new suction surface.

With the BLRS on (fig. 15), again there was a significant difference at $Q = 33$ psf, where the new suction surface TI value was lower, similar to the BLRS off case above. At the two highest Q settings, the TI values were higher for the new suction surface. Because the BLRS system did not significantly change TI for the new surface (fig. 12), the difference in figure 15 is due to the attenuating (lowering) effect on TI of the old suction surface with the BLRS on. The spectra at low Q (33 psf) and high Q (about 120 psf) are shown in figures 16(a) and (b), respectively. In figure 16(a), the large difference in TI can be seen across most of the measurement spectrum. The major difference at high Q , in figure 16(b), occurs in the spectra below 10 Hz (similar to BLRS off below 7 Hz) except for the peaks above 1000 Hz. The high-frequency peaks, however, are at amplitudes 100 to 1000 times lower than the low-frequency fluctuations. The reason for the increase (with the new suction surface) in the spectrum levels at low frequencies when the BLRS is off or on is not clear. It may be related to the change in the surface geometry over the BLRS cavity and any associated low-frequency acoustics effects.

Flow Quality Survey Test

During the flow quality survey test, TI was measured over a range of free-stream dynamic pressures at various heights and streamwise locations with the new suction surface in place. The data are presented as such: First, we discuss general features, including known factors that affect the data at all measurement locations and some common features in the frequency spectra. Second, we show the variation of TI with respect to vertical location in the test section at two streamwise locations. Finally, we show the streamwise variation of TI in the test section at three vertical locations.

General Features

Known factors common to all the data, regardless of measurement location, are: influence of the supporting cables, contribution of the instrumentation noise floor, presence of 60-Hz noise, and appearance of the wind tunnel fan blade passage frequency (BPF) in the spectra. Features common to the frequency spectra include recurring spikes in the 70- to 300-Hz frequency range and some small, higher frequency spikes.

To make measurements at multiple locations, a full-span rake was developed that could be positioned at different stations in the test section. The rake was supported at both ends by the wind tunnel walls and also had two sets of supporting cables attached to the floor and the ceiling (fig. 2(b)). In order to determine if the cables and their attachment brackets were influencing the flowfield, some data points were repeated with either the north or south side set of cables removed. Due to safety considerations, the tunnel could only be operated up to $Q = 70$ psf when the cables were removed.

Influence of the cables on measured TI is shown in figure 17(a) where the cables designated “north” were on the tunnel’s north side, and those designated “south” were nearer the tunnel’s south side. The hot-wire probe was located laterally between the north and south cables, 59 in. from the north cables and 23 in. from the south cables. As seen in the figure, removing the cables and brackets from the full-span rake did have an impact on measured data. Thus, values and trends measured and reported for the tunnel were influenced, to some degree, by the cables and brackets. Spectra are shown in figure 17(b) for $Q = 34$ psf for the three cable configurations. The effect of removing the cables appears as an amplitude shift in the spectrum’s logarithmic plot. While some of the data comparing cables off to cables on displayed slight changes with frequency, the predominant effect was the shift in amplitude with spectra exhibiting similar trends and peaks with frequency.

Because the tunnel could not be operated at a Q higher than 70 psf with the cables removed, it is difficult to predict the effect the cables were having at higher Q values. The slope of the data for all cables connected increases at the $Q = 60$ psf point. To try to determine if this was a cable phenomenon, the data were compared with TI data taken at the 14- by 22-Foot Subsonic Tunnel in 1985 (ref. 7). The measurement bandwidth at that time was the same as for the current test, 1 to 10 kHz. The data were measured at the centerline of the tunnel at the same longitudinal location with a completely different apparatus. The plot in figure 18 allows for a comparison with data taken during the current experiment at $X = 17.75$ ft and $Z = 87$ in. with the BLRS off. The 1985 data exhibit the same trend of an increasing slope of TI values at higher Q .

In general, the influence of the cables and brackets is to raise the measured TI. When the south cables (closest to the hot-wire probes) were removed, the TI values were generally lower, with an average difference of 6 percent. The largest difference was 18 percent. Note that the uncertainty in the hot-wire measurements, discussed in the appendix, is 9.4 percent. Thus the difference, where measured, is usually within the uncertainty of the measurement. Trends with the south cables removed mirror that of all the data with cables on. At higher Q values, the data from 1985 indicate that the current data trend is consistent even with the presence of cables and brackets. However, because there is a measurable effect due to the presence of the cables, wherever possible the data are presented showing the values for cables on and cables off.

Aside from the influence of the cables on measured TI values, three other factors influence all measured spectra. First is the noise floor of the instrumentation, second is the presence of 60-cycle noise, and third is the presence of the BPF.

The effect of the noise floor of the instrumentation was presented during the suction surface discussion. However, the setup for this portion of the test was substantially different from the suction surface study, so it was important to recheck the noise floor. Because the center of the front bay is where model testing is usually performed, the spectra of the voltage signals at $Q = 60$ psf, with the BLRS off and on, versus the “no flow” spectrum are shown for that test location in figure 19. Some residual flow in the test section, with the tunnel off, led to an elevated level of energy in the low-frequency range of the “no flow” spectrum. The noise floor and the signal spectra overlap at around 3000 Hz. Below about 200 Hz, there exists a slight elevation in the spectral level due to the BLRS system running. It is instructive to investigate where most of the contribution to the rms velocity fluctuation exists in the spectra. Figure 20 includes results of the spectrum integration for the $Q = 58$ psf, BLRS on condition of figure 19. As shown, over half the rms fluctuating velocity comes from the spectrum below 10 Hz. About 60 percent was contained in the region below 100 Hz and 80 percent below 2000 Hz.

Also, discussed previously in the section on suction surface replacement, all spectra contain some contamination from 60-cycle noise. Although the wall or stand probes were used to remove the noise via correlation techniques, some noise still remained. In figure 19, the 60-cycle contamination can be seen. Comparing the BLRS off spectrum with that of the BLRS on shows that, as expected, the BLRS was one source of this noise. The BLRS system was powered by a 60-Hz, 1200-rpm, 900-hp motor. When the BLRS was running, the peaks at 60 Hz in the spectra were accentuated, especially for the data obtained closest to the BLRS motor location.

A common phenomenon of spectra from wind tunnel flow measurements is the appearance of tunnel fan BPF. This occurs because each individual blade creates a distinct disturbance in the flow as a result of the wake shed as it rotates. The resulting periodic fluctuations may appear at a frequency that is a function of the number of blades and the fan RPM, which is itself a function of Q ; therefore, the peak will increase in frequency as tunnel Q increases. Figures 21(a), (b), and (c) show spectra across the range of Q for probe positions at the beginning of the front bay, the center of the front bay, and the center of the back bay, respectively. From tunnel rpm data, blade passage frequencies, based on nine fan blades, were calculated as 15, 22, 28, 35, and 40 Hz for each of the five increasing tunnel Q values.

At the beginning of the front bay and the center of the back bay (figs. 21(a) and (c)), below about 30 Hz, the spectral levels for $Q = 97$ psf are higher than those for the highest $Q = 132$ psf. One feature common to all spectra is a group of frequencies between 70 and 300 Hz, similar to those detected during the suction surface replacement study using the stand wire. These spikes are seen in figures 21(a), (b), and (c), which show the spectra at each longitudinal measurement station. (For comparison with the previous stand-mounted data, see fig. 11(b).) Spectra obtained with the hot-wire probe mounted in the survey rake are very similar to those measured using the stand. Because the two structures that held the wires were physically very different, it is likely that the spikes are representative of wind tunnel flow. However, it is still possible that some of the spikes may be associated with the natural frequency of the support. In fact, some peaks were found to be almost exact integral multiples of several of the known first five natural frequencies of the survey rake.

Similar to the suction surface study, several small peaks exist in the higher frequency range of spectra above 1000 Hz (see fig. 11(b)). Two of these peaks are seen to increase in amplitude as the aft end of the test section is approached (figs. 21(b) and (c)). This may imply that some high-frequency disturbances were propagating forward from the diffuser. Clearly the peaks detected while using the stand are stronger than those detected while using the survey rake. This may be because the stand was 13 ft downstream of the aft-most survey-rake longitudinal station, that is, closer to the diffuser section. In contrast to data from the suction surface study, some peaks appear to increase in frequency with increase in Q . While these spikes are an interesting feature of the spectra, their amplitudes are 2 to 3 orders of magnitude below the lower frequency regions of the spectra.

Vertical Variation of TI

TIs are first examined relative to vertical positioning of hot-wire probes in the test section. Shown in figure 22(a) is the variation of TI with Q at the beginning of the front bay ($X = 7.87$ ft) with the BLRS off. Data for three heights are shown, $Z = 51$, 87 (center of tunnel), and 123 in. from the floor. As shown, the TI values peak around the midrange in Q and are highest near the floor and lowest near the ceiling. There is some crossover at the two higher stations at $Q = 50$ psf. Similar trends are shown with the BLRS on in figure 22(b). For $Z = 51$ in., data obtained with the south cables removed are included in the figure. Deviation in the TI due to influence of the cables at this location begins at approximately $Q = 50$ psf. For the two higher Z positions, TI values did not change significantly with the BLRS off or

on. An example of this insensitivity to the BLRS is shown in figure 23 for one of the higher vertical positions ($X = 7.87$ ft and $Z = 87$ in.). Spectra for the condition $Q = 77$ psf with BLRS on, where the largest difference in TI occurs between the three curves, are plotted in figure 24. At $Z = 51$ in., increase in TI is concentrated at frequencies below 100 Hz. The spectrum for $Z = 87$ in. alternates between being higher and lower than the spectrum for $Z = 123$ in., with the net effect being that TI values at $Z = 123$ in. are lower.

In the center of the front bay ($X = 17.75$ ft), two vertical positions were studied. Figure 25(a) includes data with the BLRS off. Data with the cables removed are provided for $Z = 87$ in. Below $Q = 70$ psf, TI values for the probe at $Z = 87$ in. are higher than at $Z = 51$ in., and lower at higher Q value, (although the differences are close to the measurement uncertainty). At higher Q , the data obtained closest to the floor again contain the highest TI values. The same trend is evident with the BLRS on, as shown in figure 25(b), except the crossover is at $Q = 55$ psf. Similar to the previous X station, the BLRS, when operating at high Q values, seems to have affected the data at lower vertical positions ($Z = 51$ in.) more than at higher vertical positions ($Z = 87$ in.), as shown in figure 26. The difference in the spectra, due to the change in Z (vertical) position, at this X location at the highest Q is shown in figure 27. As before, the major difference occurs below 100 Hz and shows a clear increase at the lower height ($Z = 51$ in.).

Streamwise Variation of TI

The effect of longitudinal position is examined at three heights: $Z = 51$, 87, and 123 in. In figure 28(a), at $Z = 51$ in. with BLRS off, TI values at the beginning of the front bay ($X = 7.87$ ft) are equal to or higher than those at the middle of the front bay ($X = 17.75$ ft) until a Q of 80 psf is reached. This would be the expected trend in absence of any mean velocity gradient. Above $Q = 80$ psf, TI values diverge rapidly and downstream TI increases significantly over the upstream value. The cause for this is unknown. With the BLRS on, the same trend occurs (fig. 28(b)) with the crossover at a slightly higher Q . Spectra at the largest divergence, above $Q = 130$ psf, with the BLRS off and on, are shown in figures 29(a) and (b), respectively. In this case, moving the probe longitudinally downstream at a fixed height, at the highest Q , increases the spectral levels across the full measurement frequency range. This effect is independent of whether the BLRS is off or on. Note that increase in the spectral level only appears uniform due to the logarithmic vertical scale. Actually, the largest increases are concentrated in the frequency range below about 10 Hz, as shown in the semilog plot in figure 29(c).

Figure 30(a) includes the same two longitudinal locations, $X = 7.87$ ft and $X = 17.75$ ft, in the middle of the tunnel vertically, $Z = 87$ in., with the BLRS off. The trend at high Q values is the same as for $Z = 51$ in. However, at Q values in the lower range, TI values at the middle of the model cart ($X = 17.75$ ft) are still higher. TIs for the two longitudinal locations are equivalent between a Q of 60 and 80 psf. With the BLRS on (fig. 30(b)) TI values at $X = 17.75$ ft are always higher, except between a Q of 60 and 80 psf, where they are still close to the data taken at the beginning of the front bay. With the BLRS on, spectra at $Q = 33$ and about 130 psf are shown in figures 31(a) and (b). As for the previous height ($Z = 51$ in.), amplitude of the spectra is higher across the frequency range at the further aft X station.

A comparison of data measured at the beginning of the front bay, $X = 7.87$ ft, and the middle of the back bay, $X = 40$ ft, at the highest vertical location, $Z = 123$ in., may be made from the plot shown in figure 32(a) for the BLRS off. No data were obtained at this height for $X = 17.75$ ft. Similar to data at $Z = 51$ in., TI at the downstream rake location is lower at Q s less than 80 psf and higher above. It is possible, however, that the TI has fallen between $X = 17.75$ ft and $X = 40$ ft given the elevated levels detected at $X = 17.75$ ft. Figure 32(b) features the same data with the BLRS operating. Cables off data

are included for $X = 40$ ft. Below $Q = 60$ psf, TI values are very close but above $Q = 60$ psf, downstream TI is again higher than that at the entrance. In figure 32(c), the TIs for BLRS off/on for $X = 40$ ft are shown. Spectra at $Q = 33$ and 132 psf, BLRS on, are shown in figures 33(a) and (b), respectively. As might be expected, there is a small difference in the spectral levels at $Q = 33$ psf because the corresponding TI values were close. At $Q = 132$ psf, most of the difference is below 100 Hz, although there is a slight increase in levels above 100 Hz for the further aft location.

Concluding Remarks

Turbulence intensities (TIs) and frequency spectra in the free stream of the 14- by 22-Foot Subsonic Tunnel test section were measured, in the closed or “walls-down” configuration, for a variety of tunnel conditions. This study was performed in support of a subsequent three-dimensional High-Lift Flow Physics (3-D HLFP) experiment using hot-wire anemometry.

In general, the turbulence levels are low. At a dynamic pressure (Q) of 60 psf, the TI is between 0.07 and 0.08 percent; however, it varies with Q and with location. The character of frequency spectra remains fairly consistent throughout the test section, changing mostly in amplitude and only slightly with frequency. All spectra have approximately half the total energy concentrated below 10 Hz. The spectra decline with increasing frequency until roughly 70 Hz, where they plateau until about 300 Hz, and contain a group of peaks that shifts in frequency with Q . The level of the spectra then declines again until it eventually merges with the instrumentation noise floor. Some small amplitude peaks exist above 1000 Hz as the diffuser is approached.

Results from the suction surface replacement study show that no significant adverse effect was manifested in the wind tunnel turbulence environment due to the installation of a new boundary layer removal system (BLRS) surface grid when the BLRS is not running. However, with the BLRS running, there was some increase in TI above a tunnel free-stream dynamic pressure, Q , of 80 psf. There were also indications of low-level disturbances at discrete frequencies above 1000 Hz in the power spectral densities in the back of the test section.

During the flow quality survey, three vertical and three longitudinal probe positions were used to survey the flow in the test section. Results of this study demonstrate that TI is a function of Q and location in the test section. Thus, the reporting of one value of TI as representative of a wind tunnel may be misleading. TI was generally found to be higher at lower vertical positions in the test section. At the lowest and highest vertical positions ($Z = 51$ and 123 in.), TIs at the beginning of the front bay ($X = 7.87$ ft) tended to be higher than the values farther downstream at Q values below around 80 psf. At higher Q values, TI values at the beginning of the front bay ($X = 7.75$ ft) were lower. At the middle vertical position ($Z = 87$ in.), TI values at the beginning of the front bay were generally always lower than those downstream. The effect of running the BLRS system during the flow quality survey was minimal on TI values, increasing them only slightly in certain locations in the mid- Q range. The effect on the spectra was a slight increase in amplitude below 200 Hz.

The flow quality survey data were affected by the full-span rake support cables and attachment brackets. Although the difference was often within the measurement uncertainty, occasionally it could be larger. Ideally, wind tunnel turbulence measurements should be made separately from all other measurements so that a support structure that creates minimal flow interference can be used. Unfortunately for production wind tunnels, this is usually cost prohibitive.

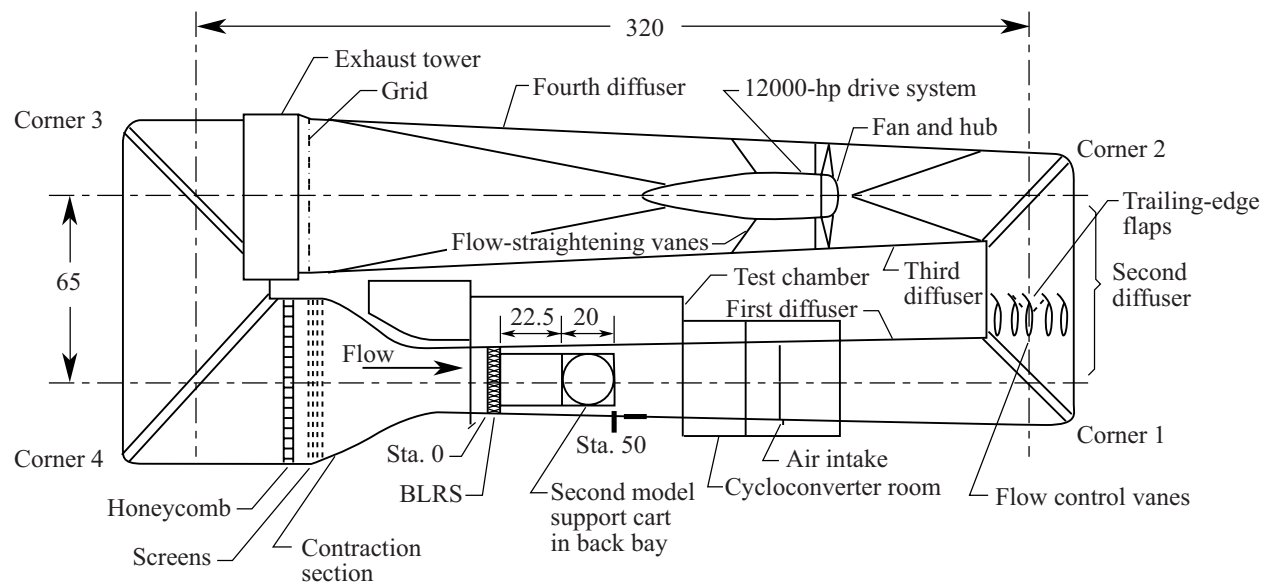
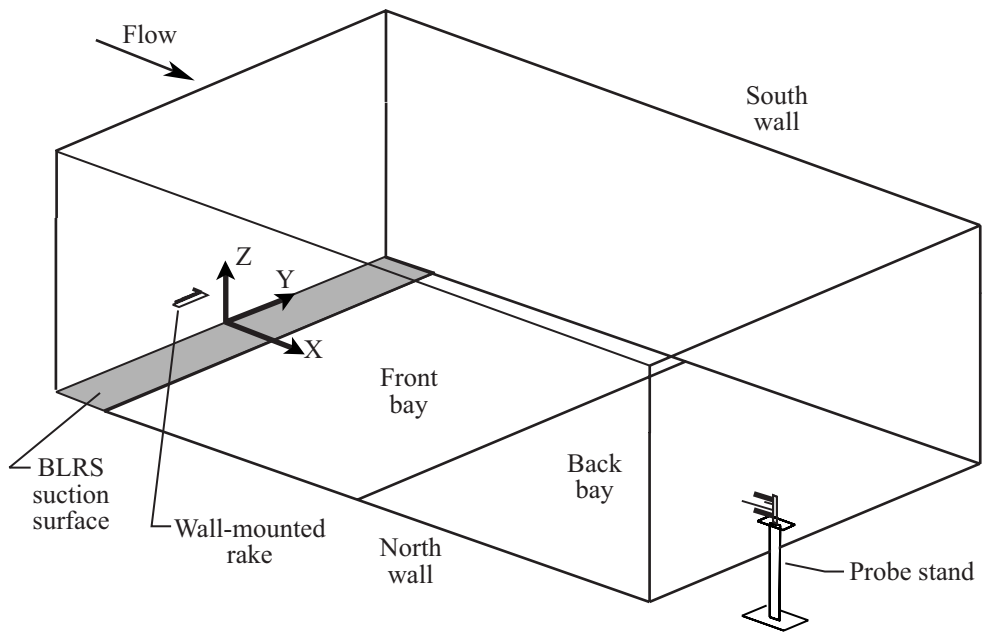
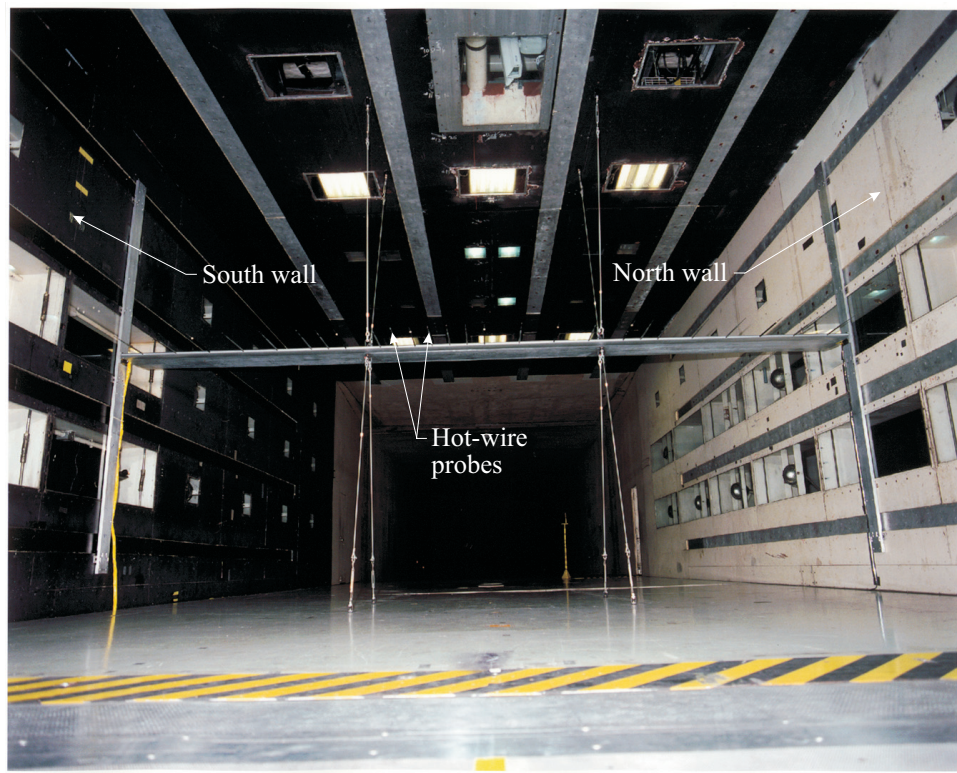


Figure 1. Langley 14- by 22-Foot Subsonic Tunnel circuit. (All dimensions are in feet.)

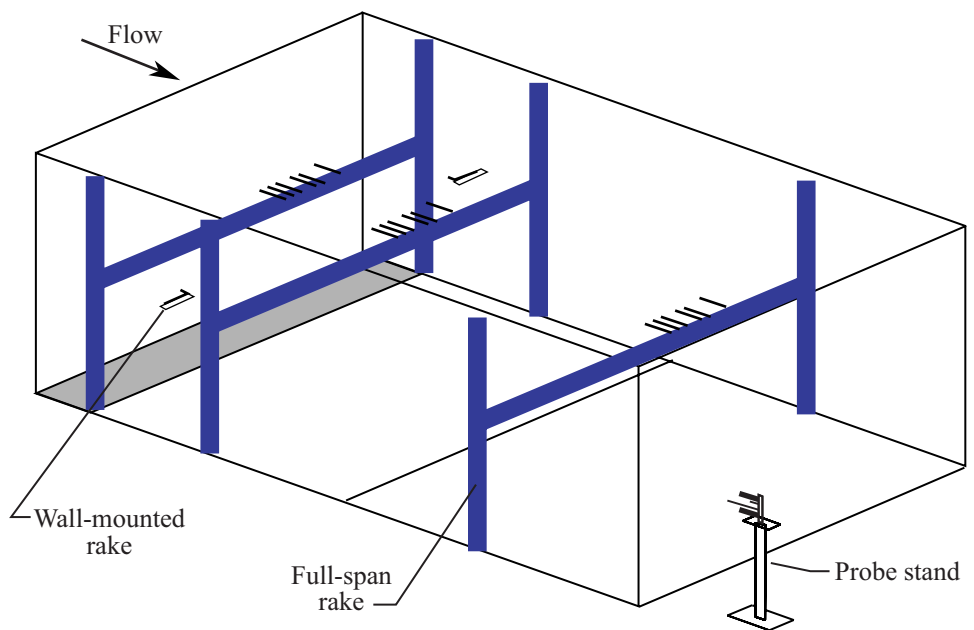


(a) Hot-wire probe layout for turbulence measurement, suction surface study.



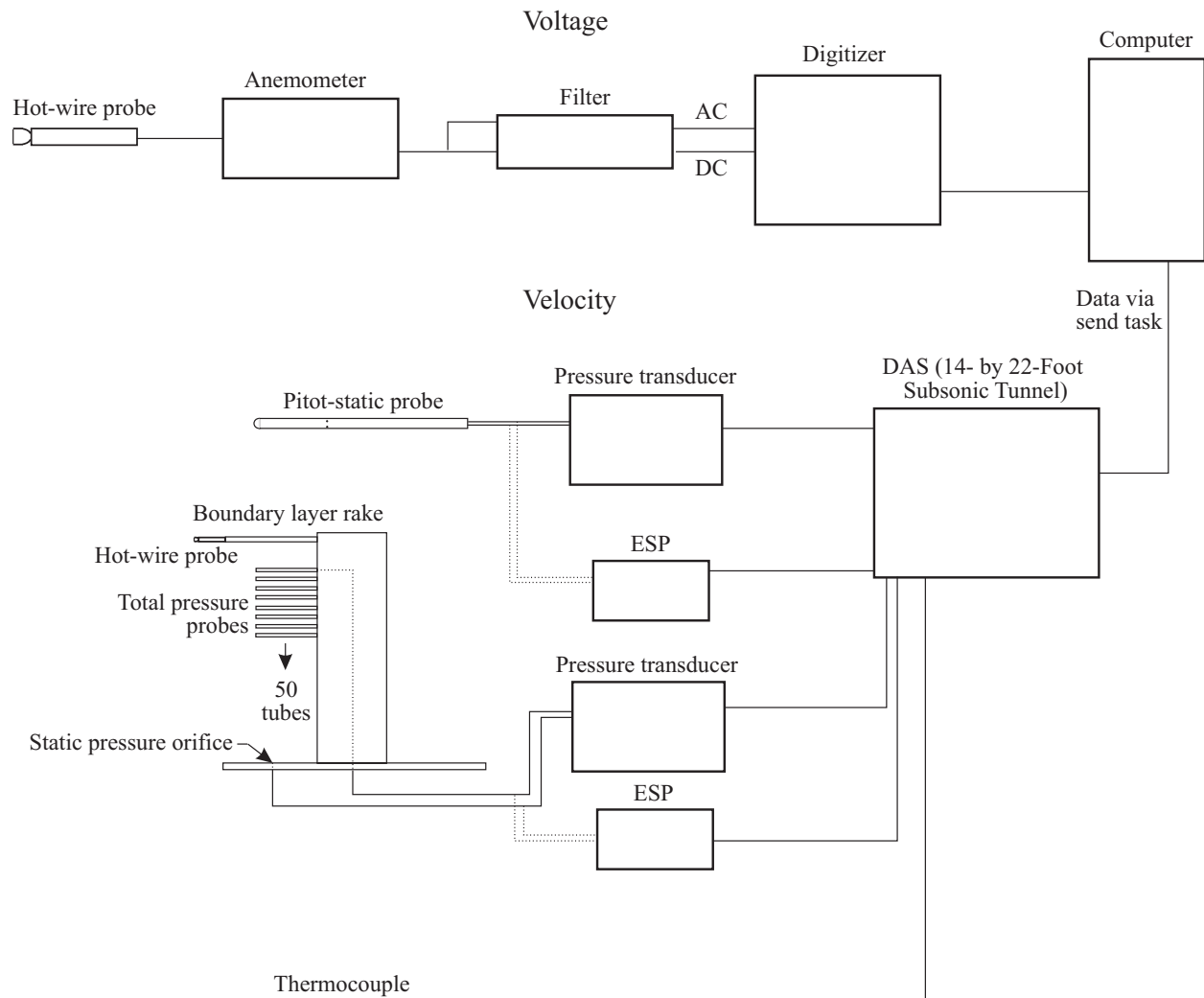
(b) Full-span rake, center of front bay.

Figure 2. Langley 14- by 22-Foot Subsonic Tunnel test section.



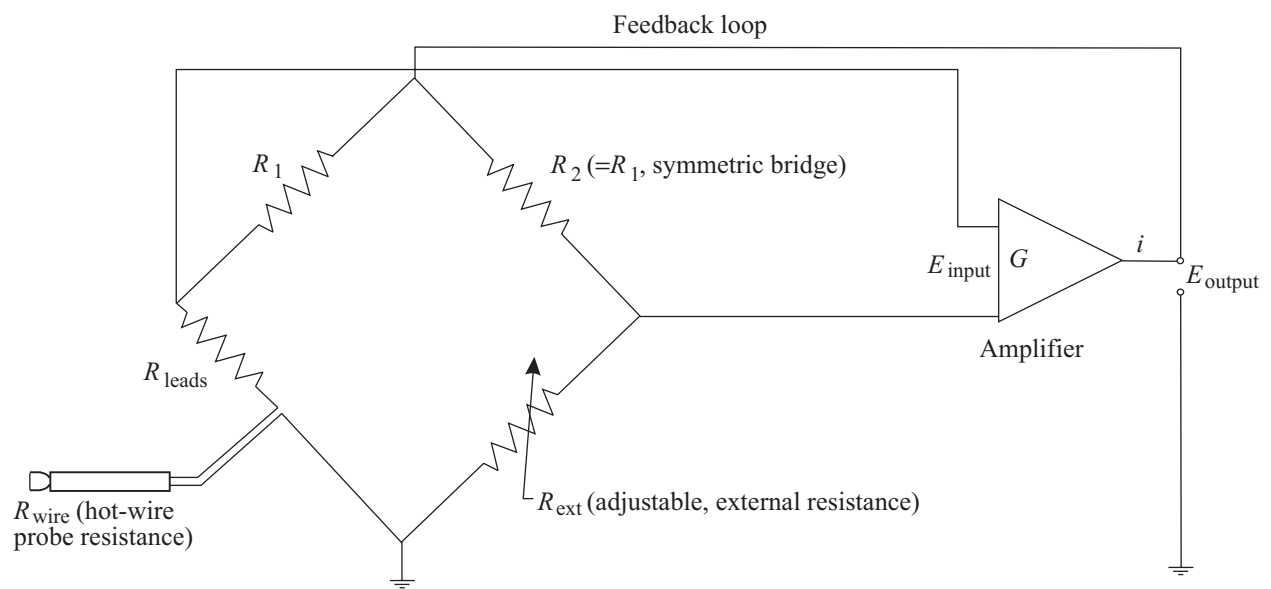
(c) Hot-wire probe layout for turbulence measurement, flow survey test.

Figure 2. Concluded.



(a) Overall setup.

Figure 3. Experimental instrumentation.



(b) Basic constant temperature anemometer circuit.

Figure 3. Concluded.

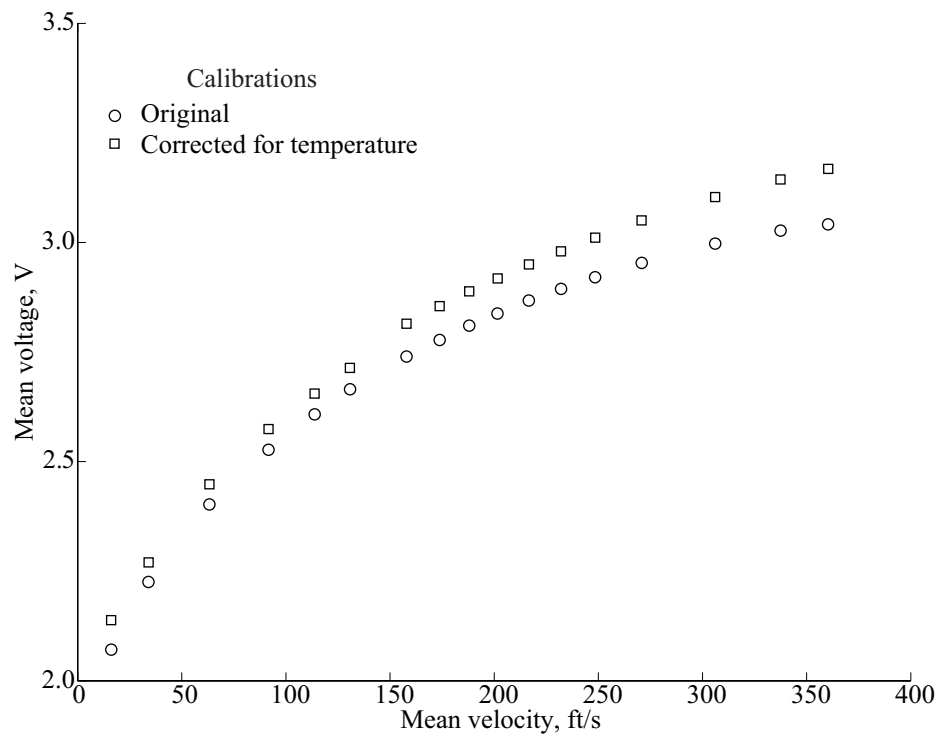


Figure 4. Langley 14- by 22-Foot Subsonic Tunnel: hot-wire calibration, corrected for temperature.

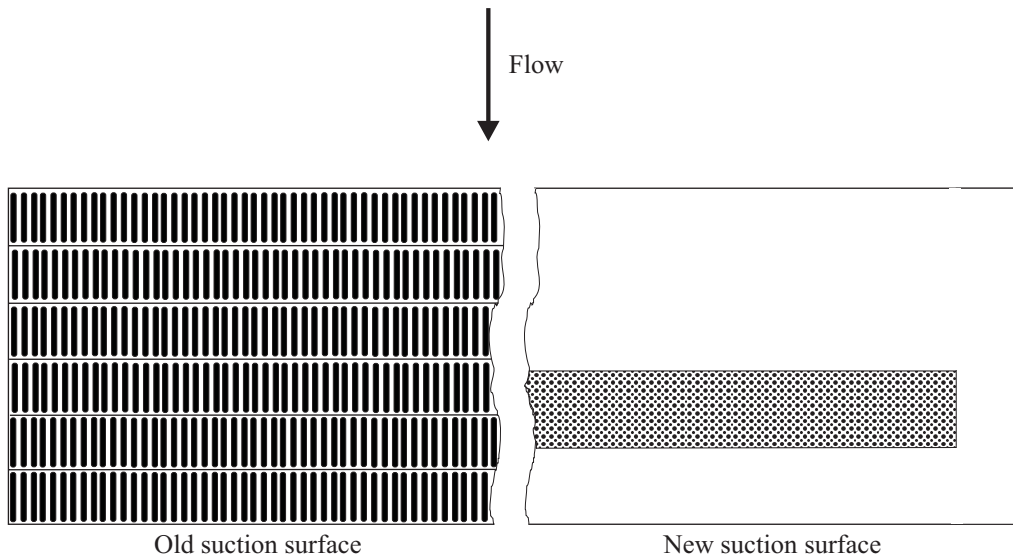
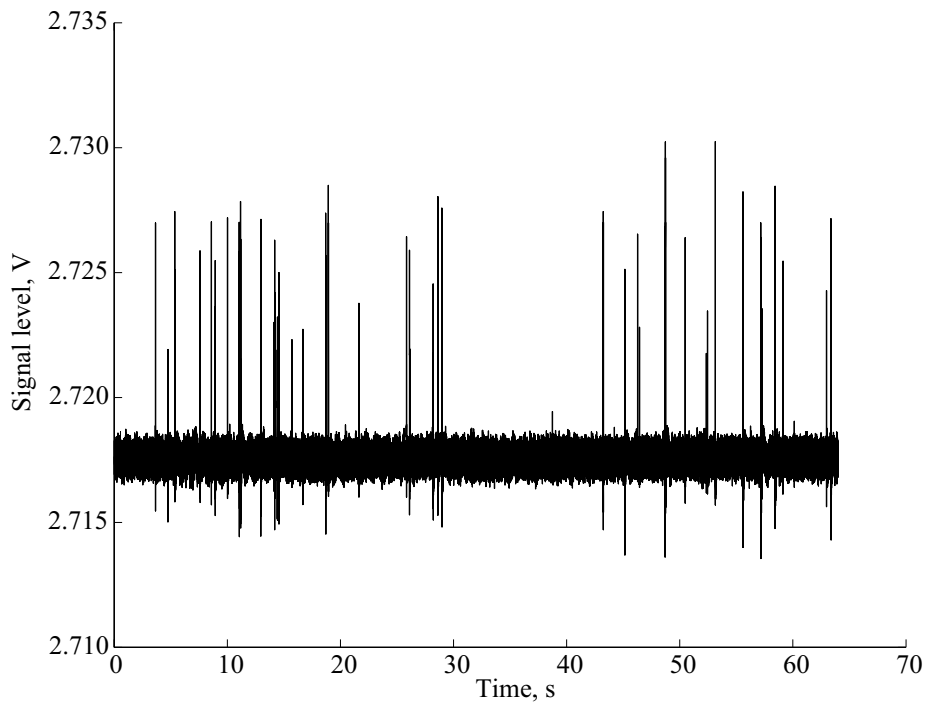
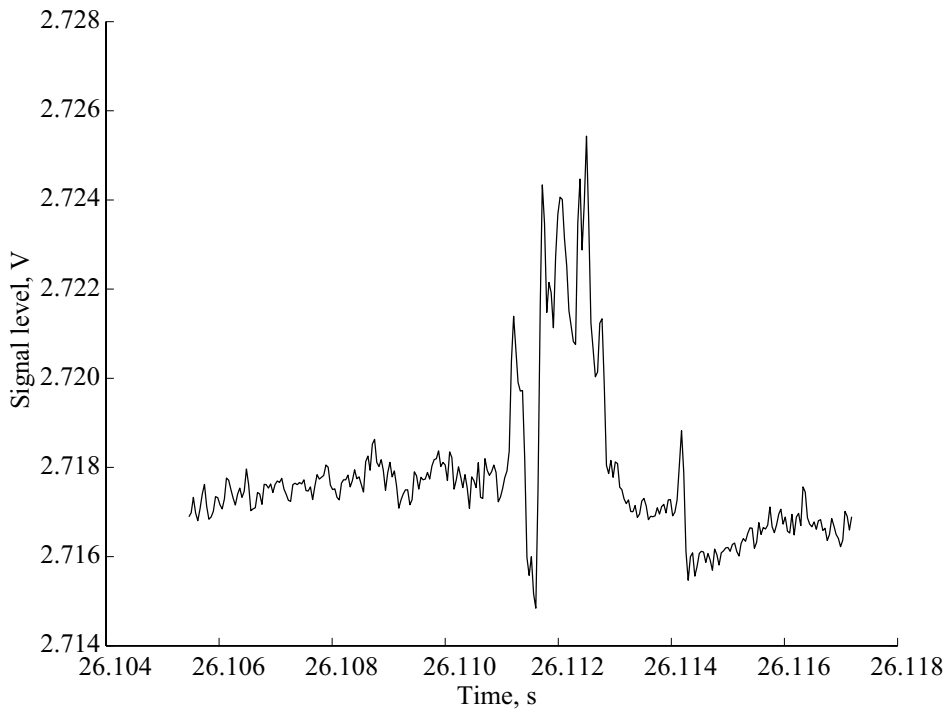


Figure 5. BLRS suction surface patterns.



(a) $Q = 60$ psf, BLRS off, wall wire.



(b) Expanded, $Q = 60$ psf, BLRS off, wall wire.

Figure 6. Langley 14- by 22-Foot Subsonic Tunnel time series.

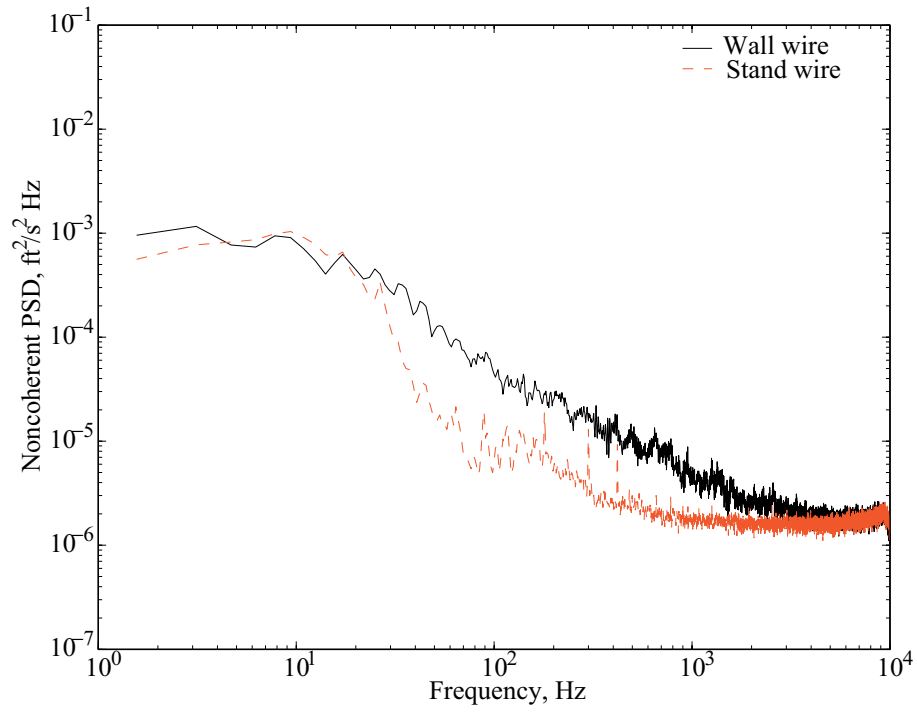


Figure 7. Langley 14- by 22-Foot Subsonic Tunnel, PSD wall wire versus stand wire, old suction surface, $Q = 59$ psf, BLRS off.

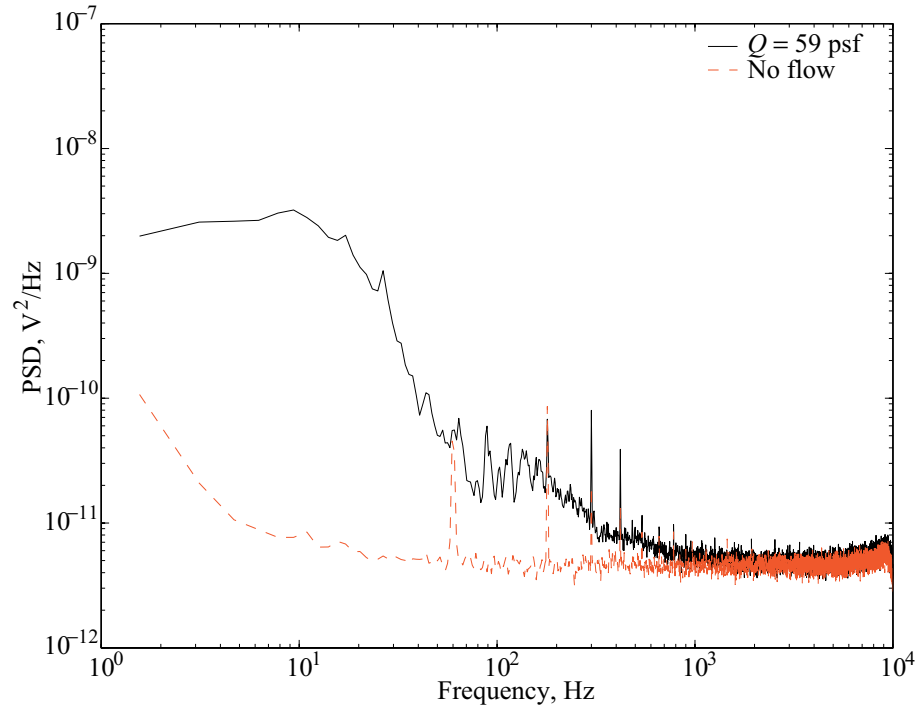
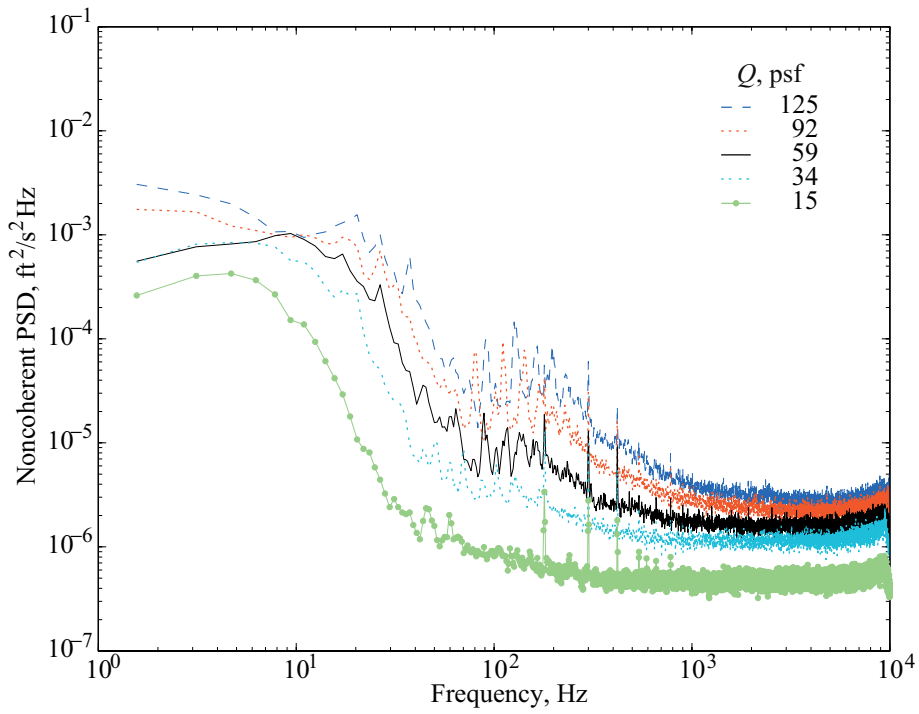
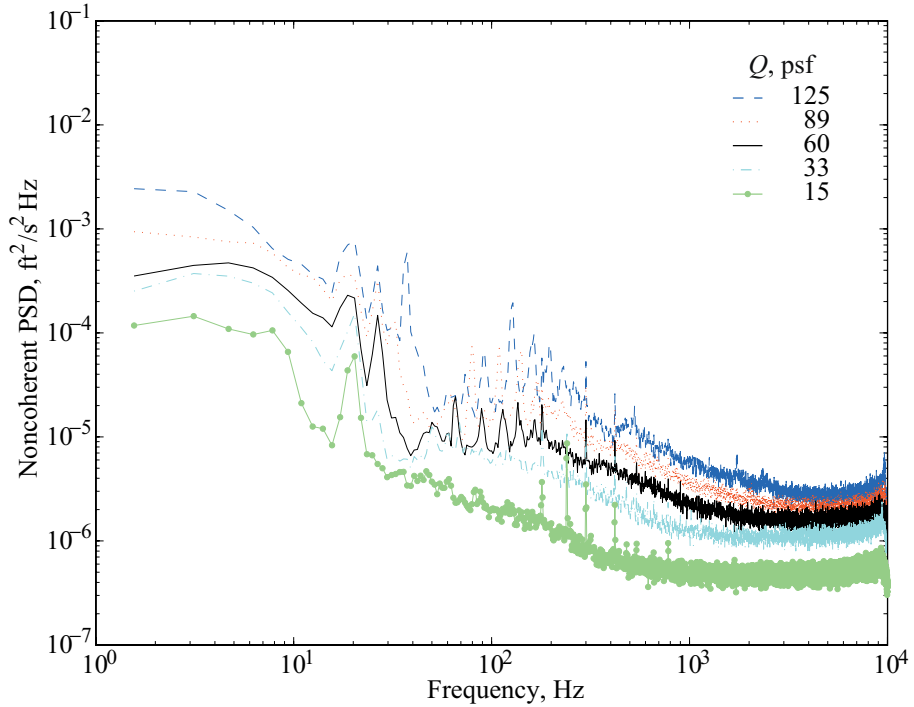


Figure 8. Langley 14- by 22-Foot Subsonic Tunnel, PSD old suction surface, stand hot-wire probe, $Q = 59$ psf versus “no flow.”

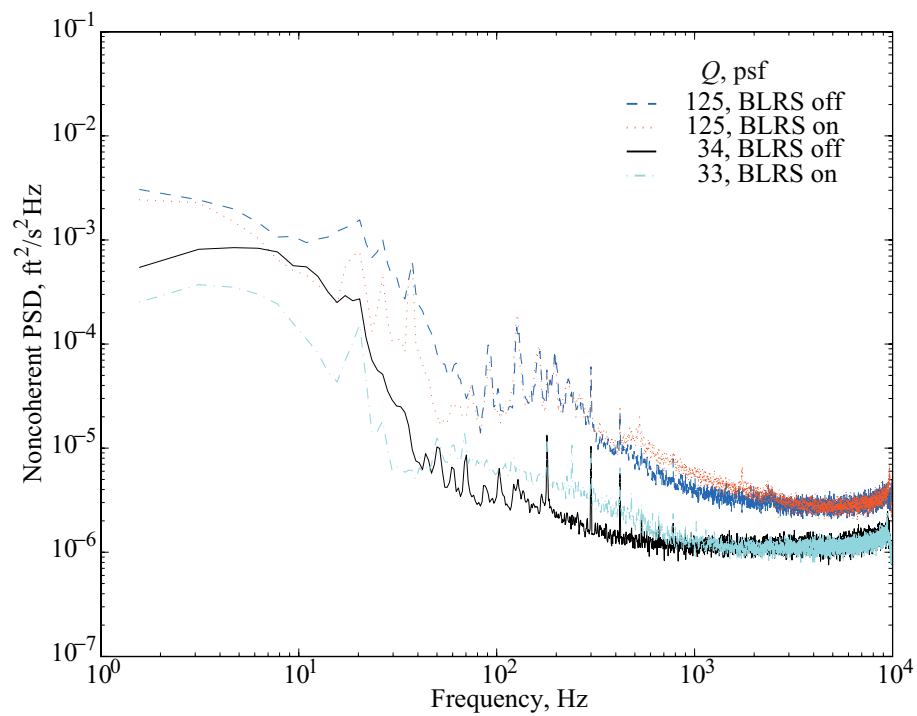


(a) Stand hot-wire probe, BLRS off.



(b) Stand hot-wire probe, BLRS on.

Figure 9. Langley 14- by 22-Foot Subsonic Tunnel, PSD old suction surface.



(c) Stand hot-wire probe.

Figure 9. Concluded.

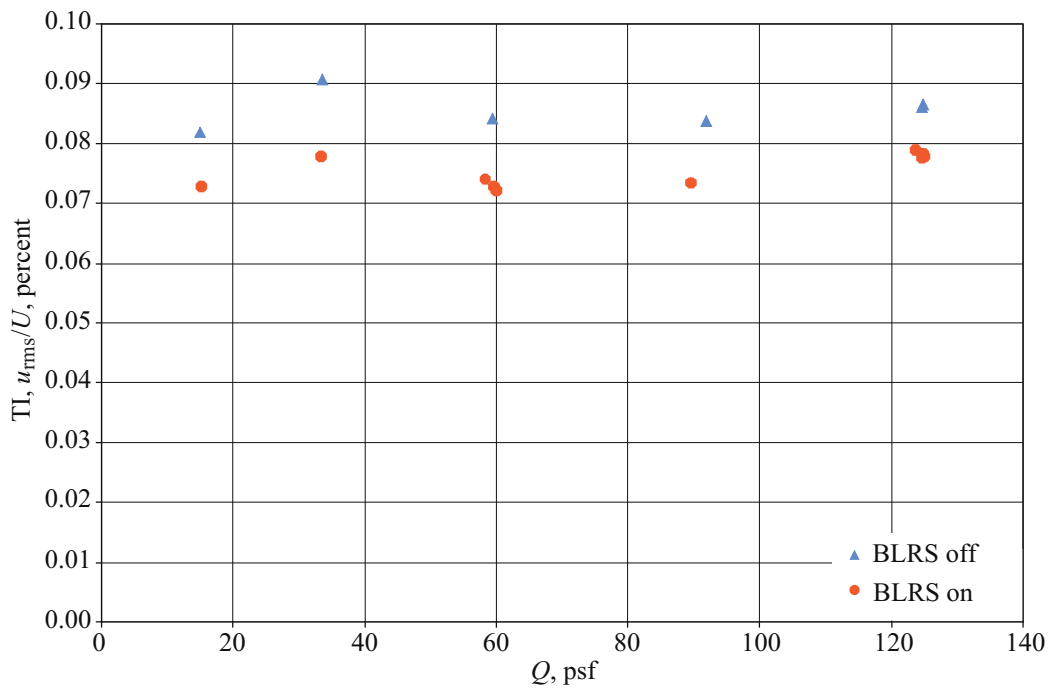
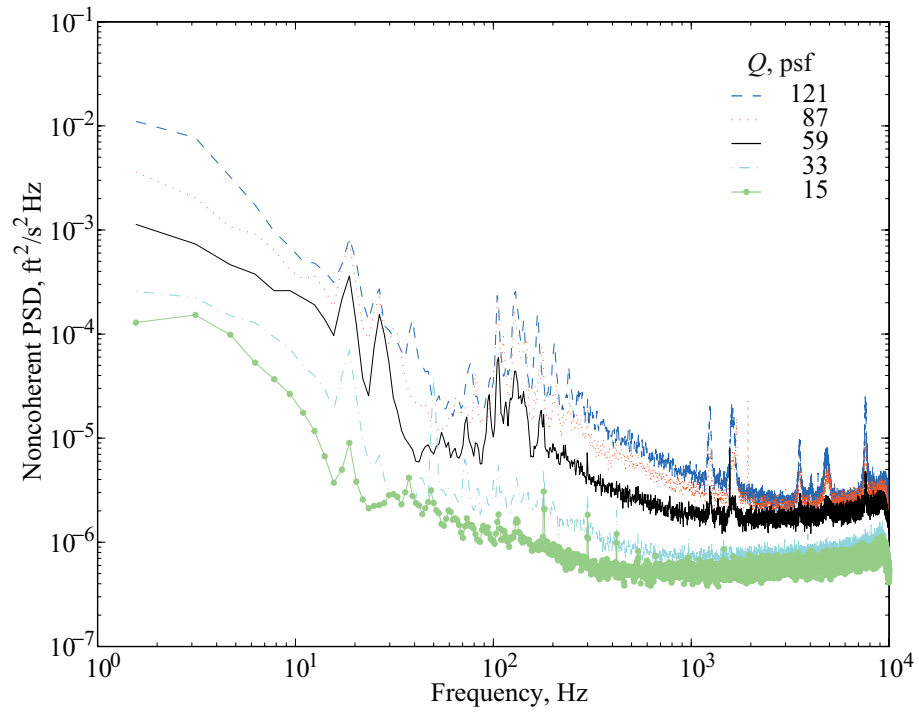
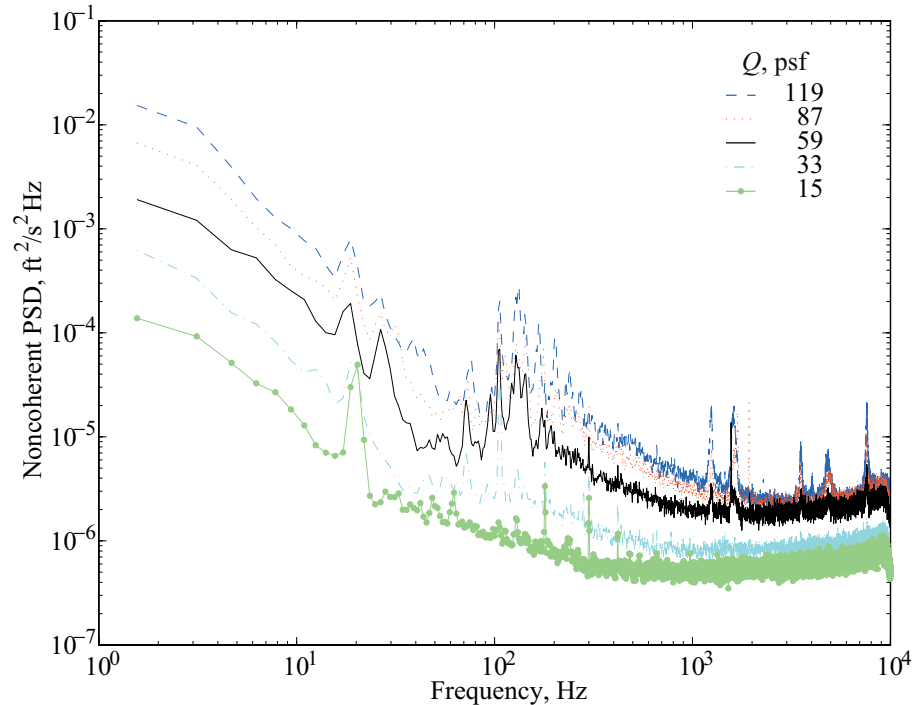


Figure 10. Turbulence intensity, old BLRS suction surface.

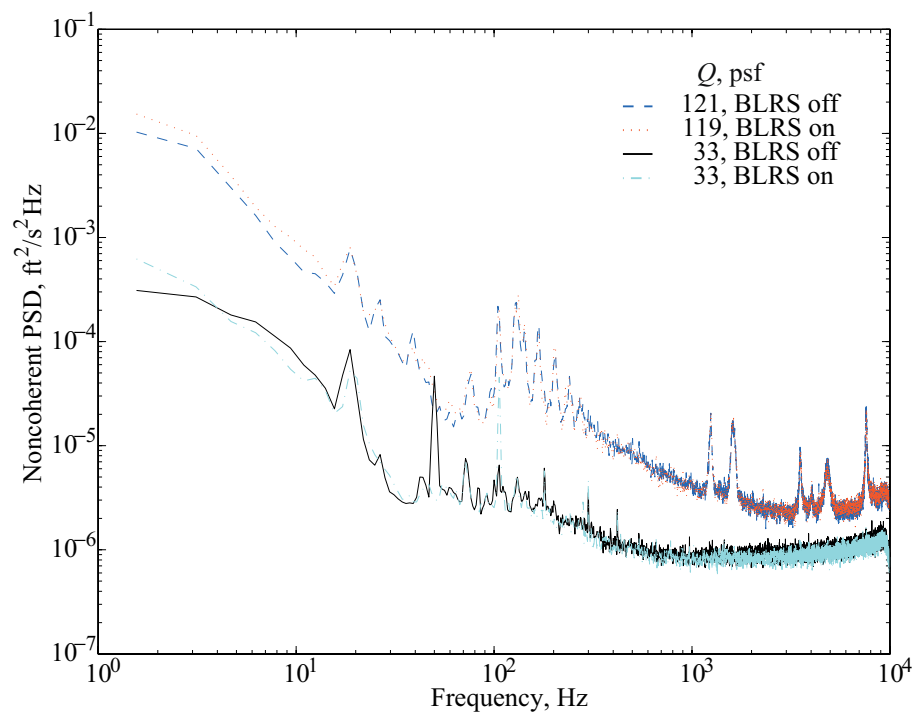


(a) Stand hot-wire probe, BLRS off.



(b) Stand hot-wire probe, BLRS on.

Figure 11. Langley 14- by 22-Foot Subsonic Tunnel, PSD new suction surface.



(c) Spectra comparison, stand hot-wire probe.

Figure 11. Concluded.

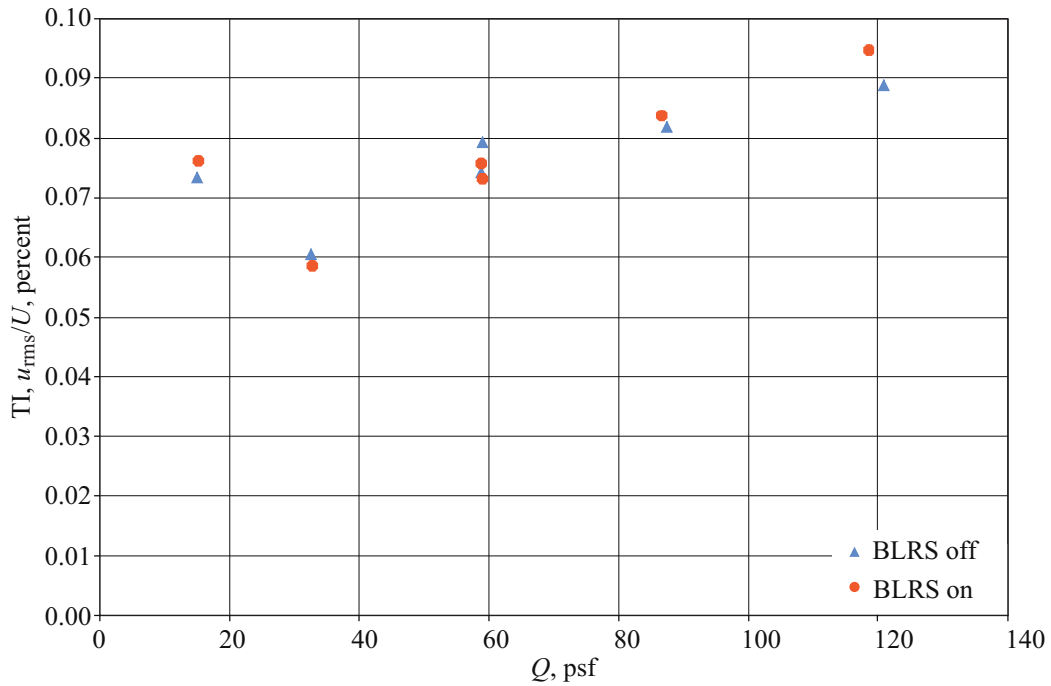


Figure 12. Turbulence intensity, new BLRS suction surface.

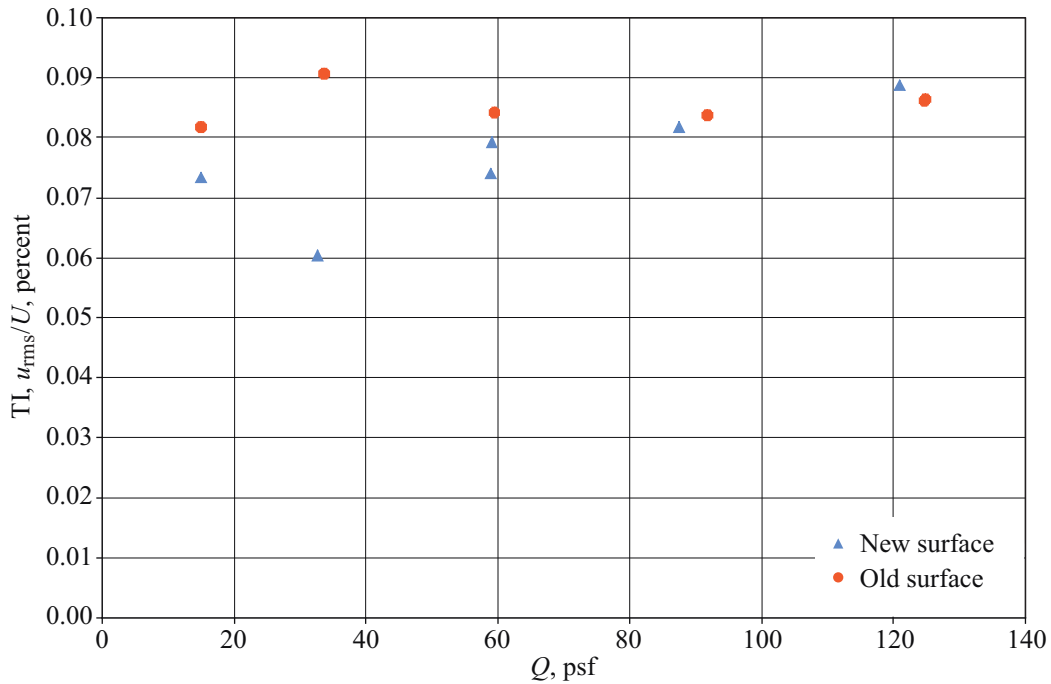
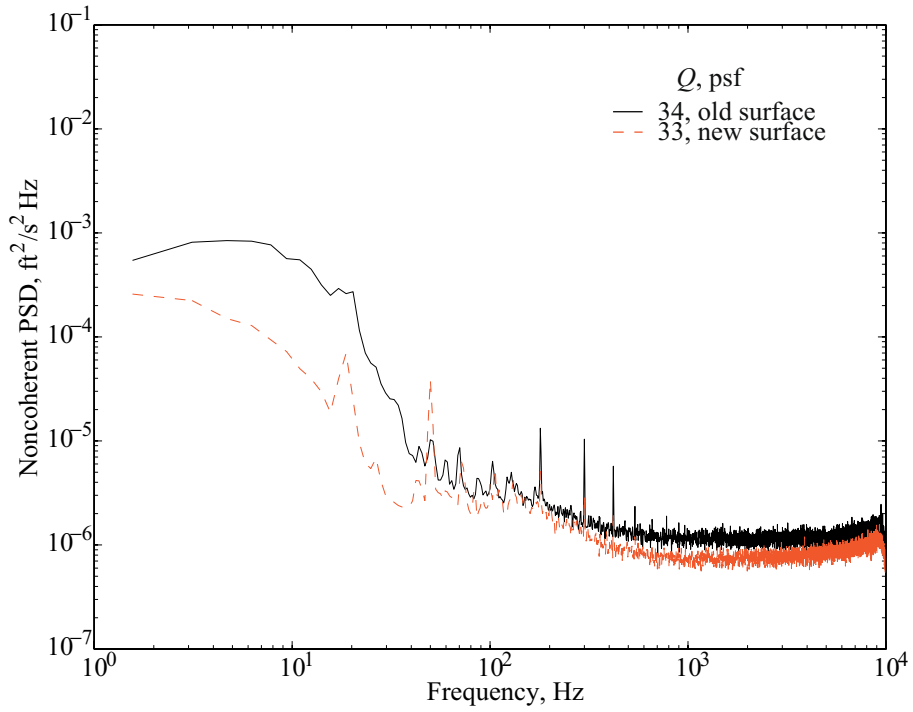
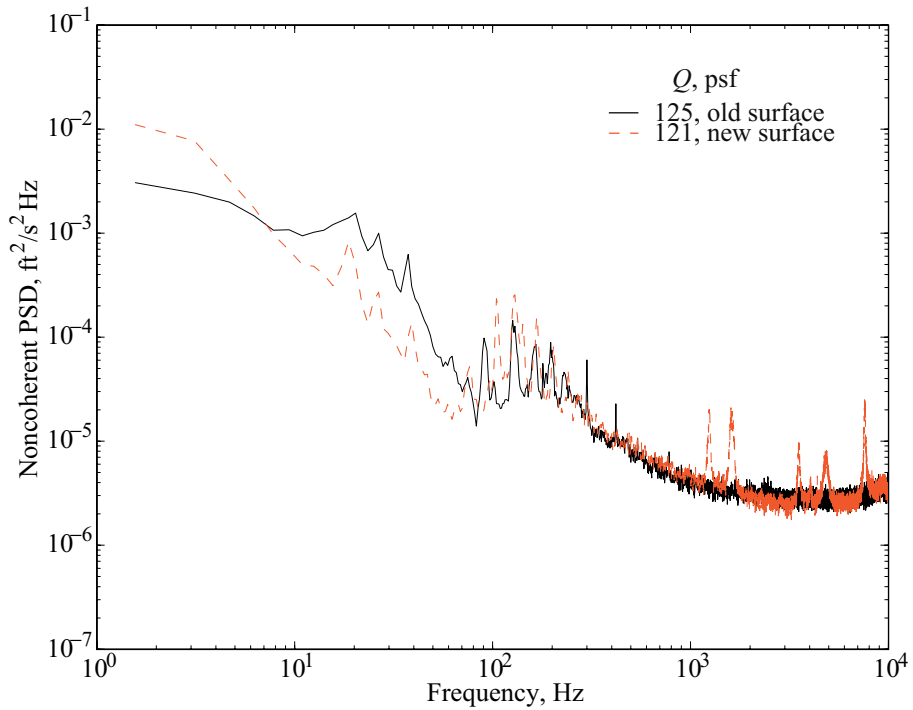


Figure 13. Turbulence intensity, new versus old suction surface, BLRS off.



(a) $Q \approx 33$.



(b) $Q \approx 120$.

Figure 14. Langley 14- by 22-Foot Subsonic Tunnel, PSD new versus old suction surface, stand wire, BLRS off.

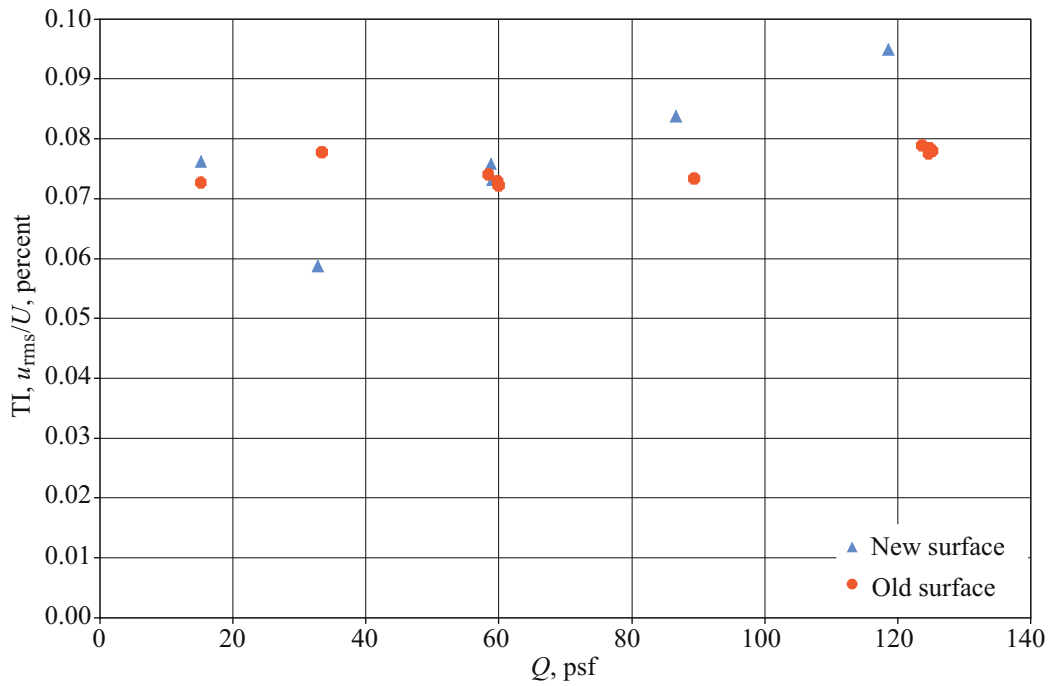
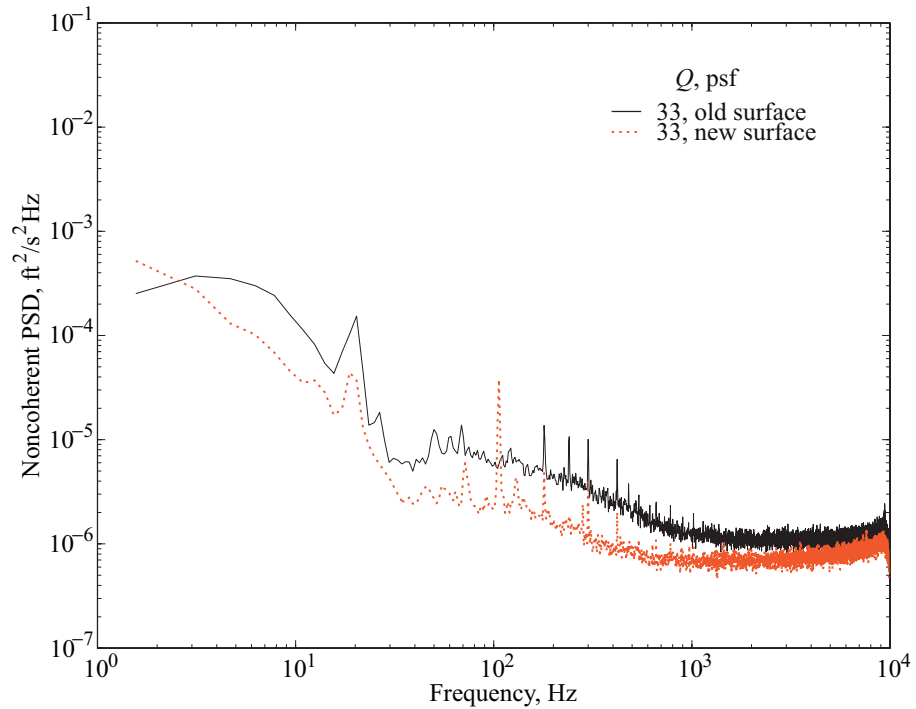
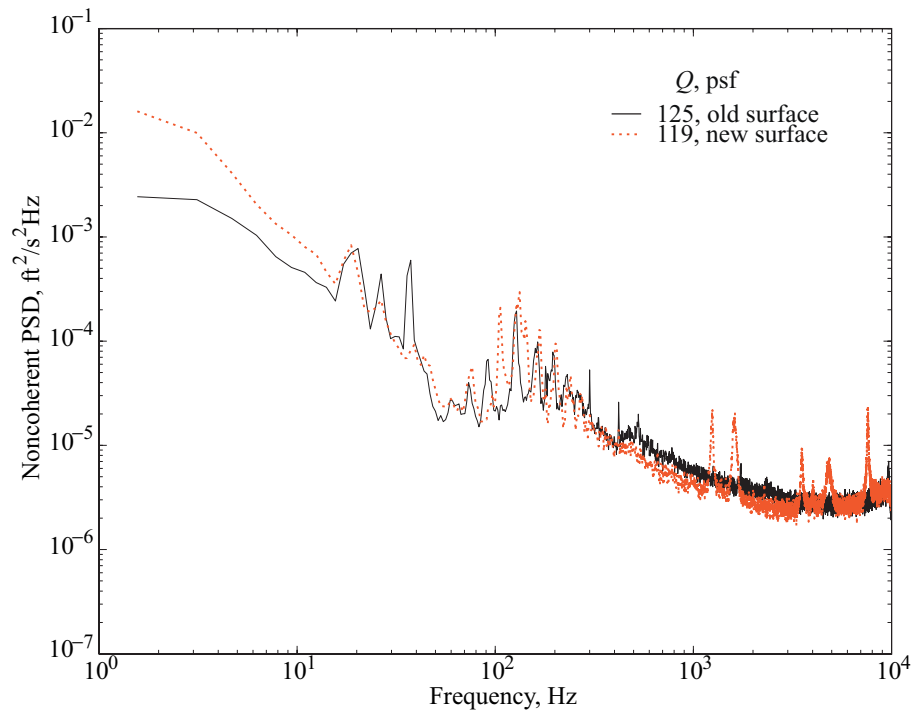


Figure 15. Turbulence intensity, new versus old suction surface, BLRS on.

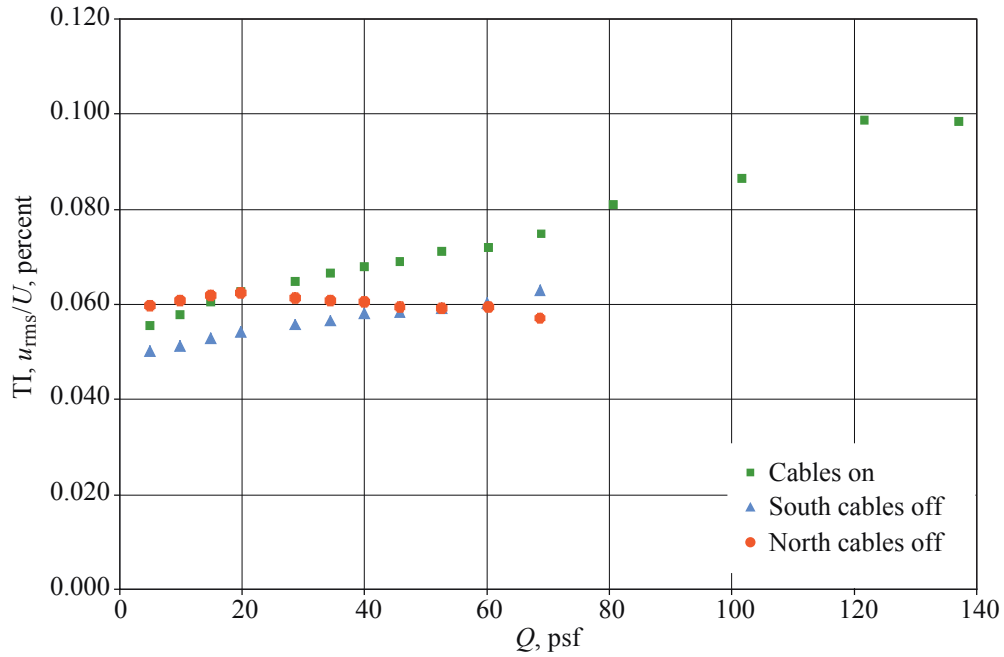


(a) $Q = 33$.

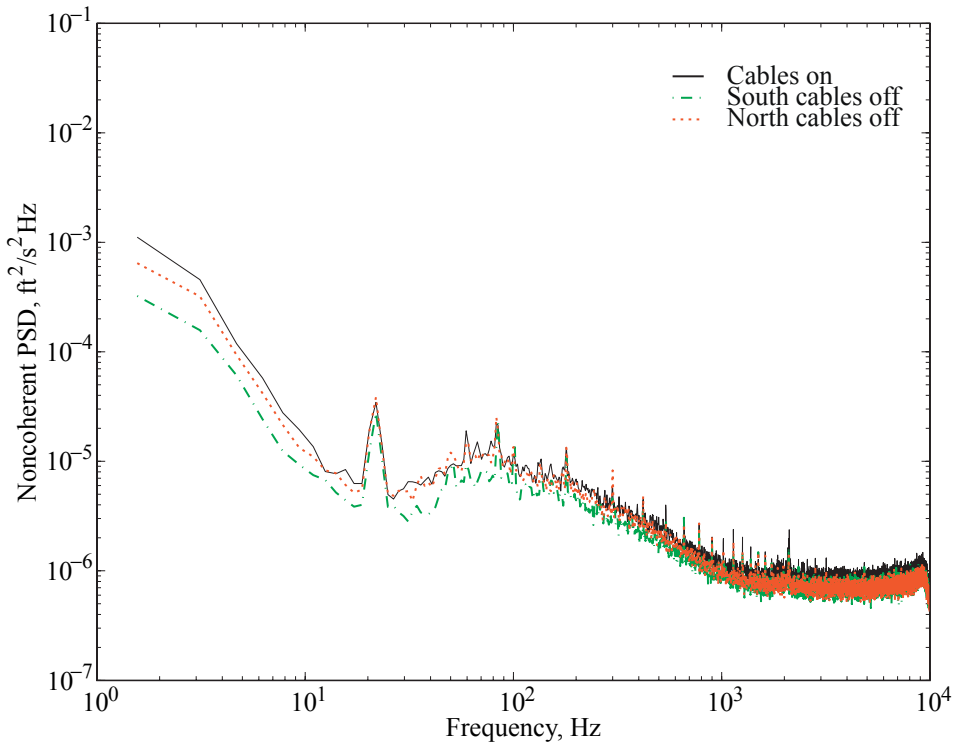


(b) $Q \approx 120$.

Figure 16. Langley 14- by 22-Foot Subsonic Tunnel, PSD new versus old suction surface, stand wire, BLRS on.



(a) Effect of cable attachment ($X = 17.75$ ft, $Z = 87$ in.), BLRS off.



(b) PSD center of front bay, probe height 87 in., BLRS off, $Q = 34$ psf.

Figure 17. Langley 14- by 22-Foot Subsonic Tunnel, turbulence intensity.

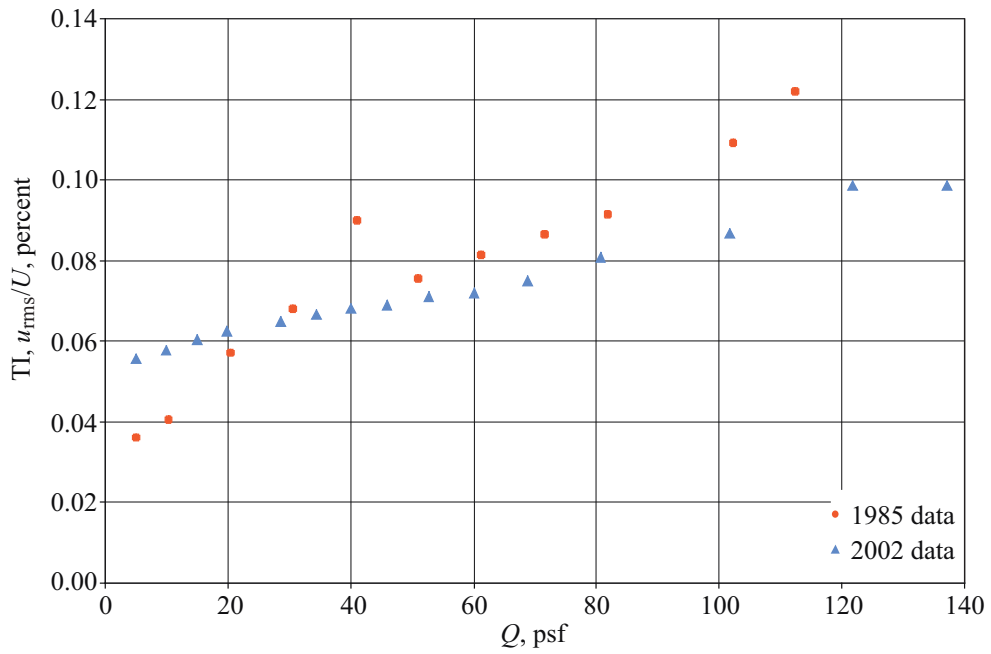


Figure 18. Turbulence intensity, comparison with previous data ($X = 17.75$ ft, $Z = 87$ in.), BLRS off.

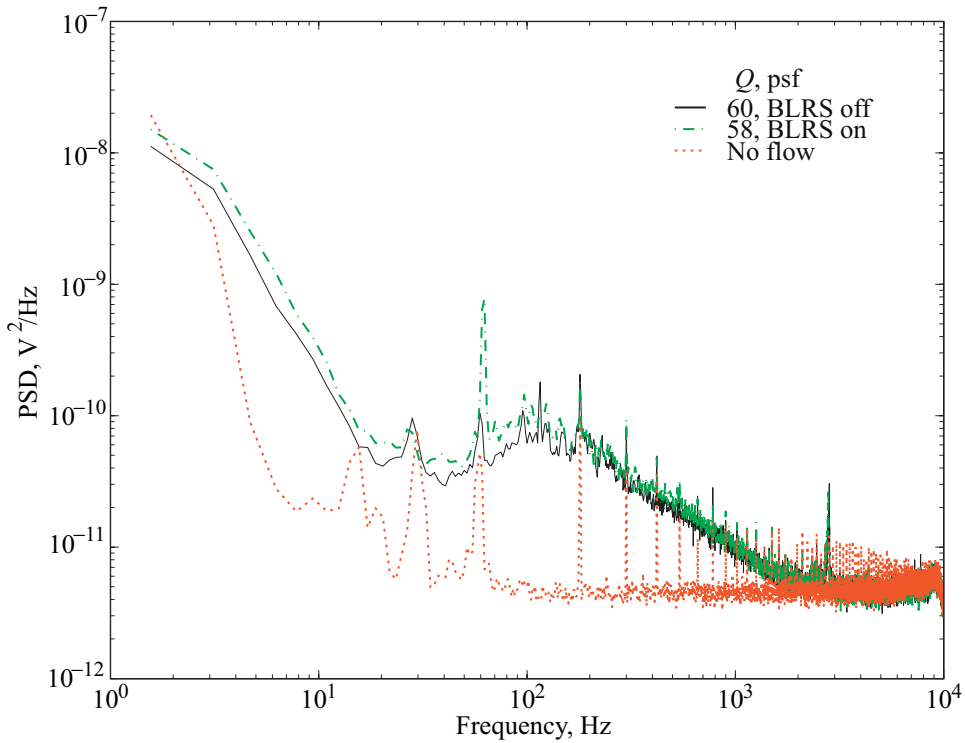


Figure 19. Langley 14- by 22-Foot Subsonic Tunnel, PSD center of front bay ($X = 17.75$ ft, $Z = 87$ in.).

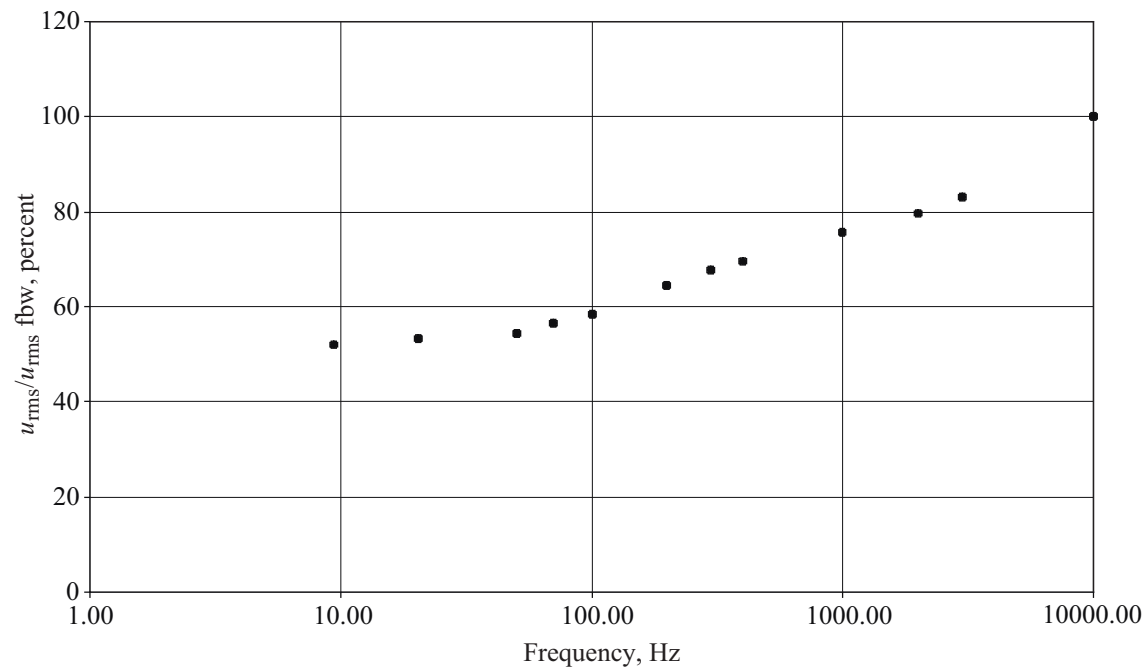
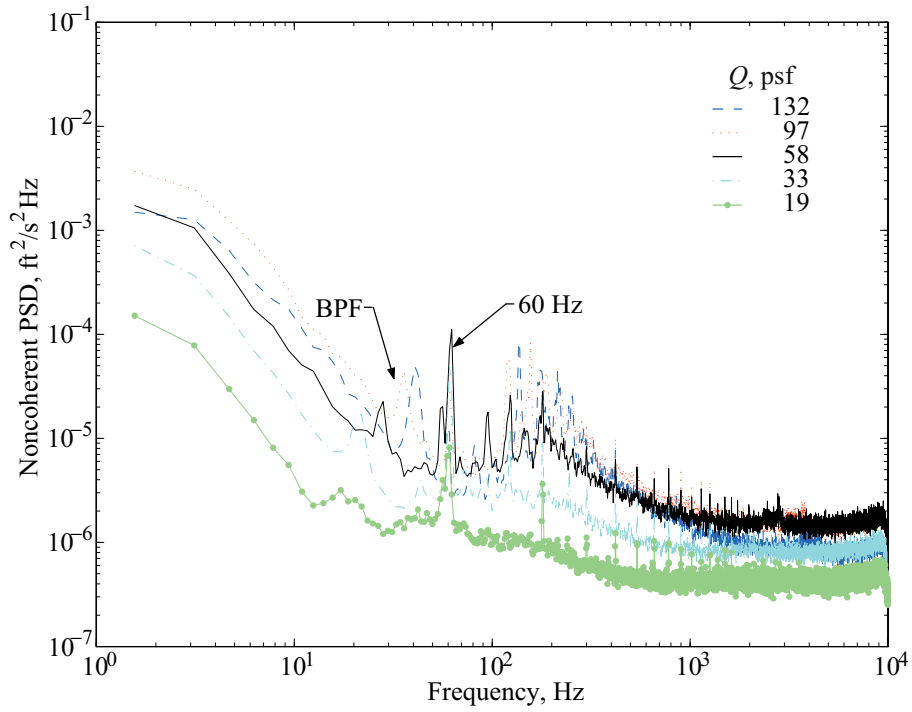
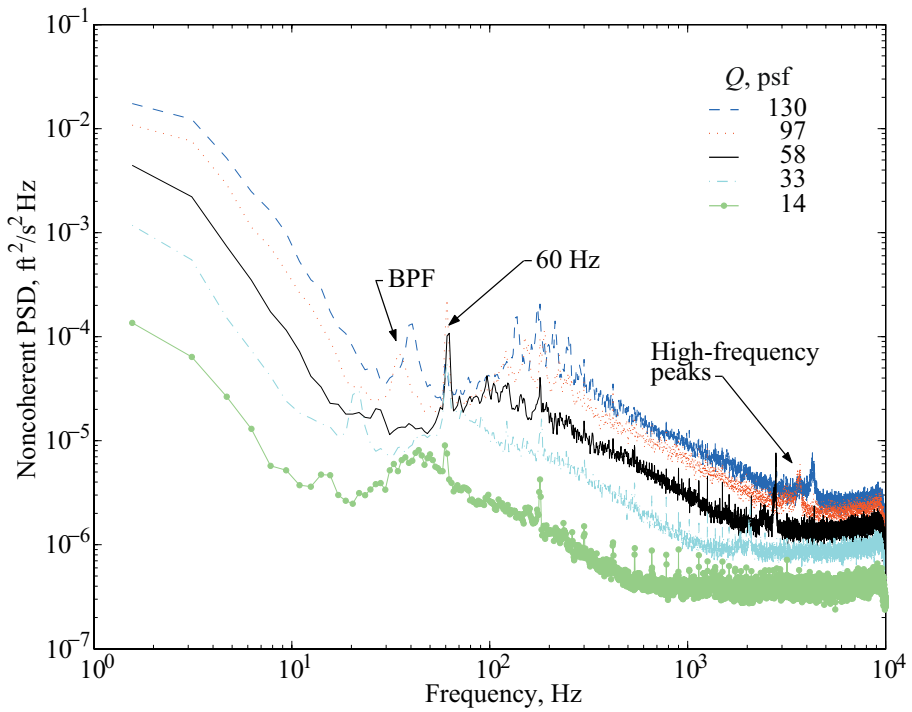


Figure 20. Effect on rms velocity of integration over less than full bandwidth; 14- by 22-Foot Subsonic Tunnel,
 $Q = 58 \text{ psf}$, BLRS on, center of front bay.

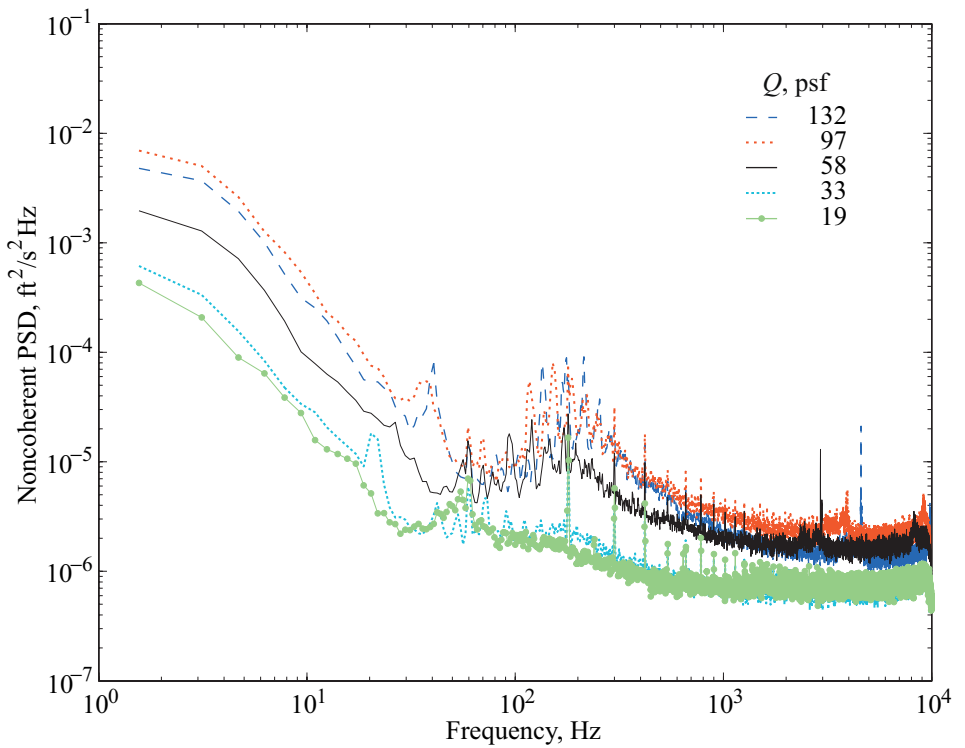


(a) Beginning of front bay ($X = 7.87$ ft, $Z = 123$ in.), BLRS on.



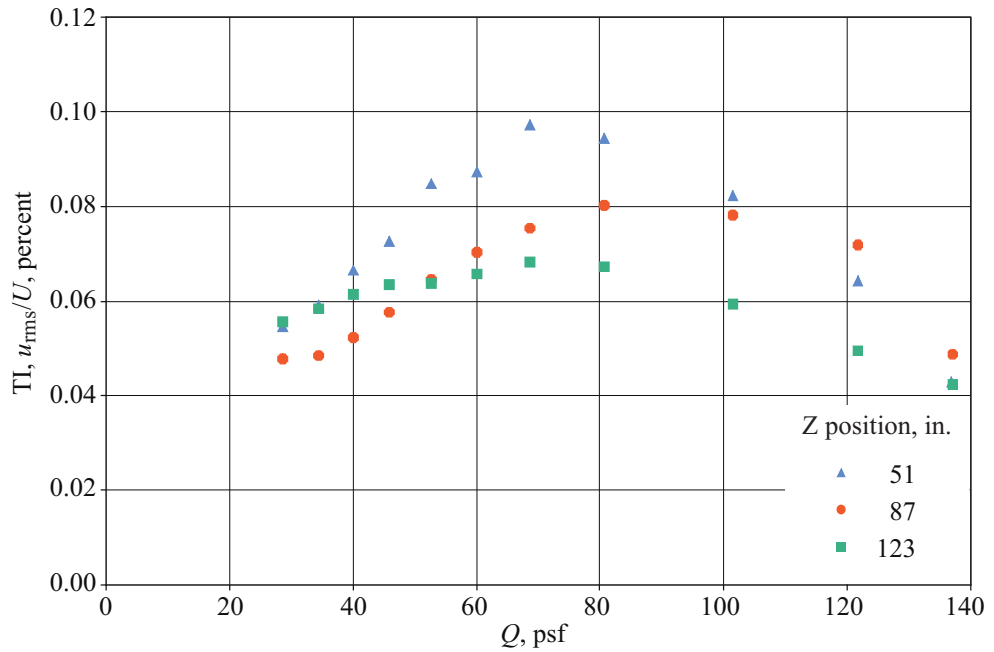
(b) Center of front bay ($X = 17.75$ ft, $Z = 87$ in.), BLRS on.

Figure 21. Bay location readings.

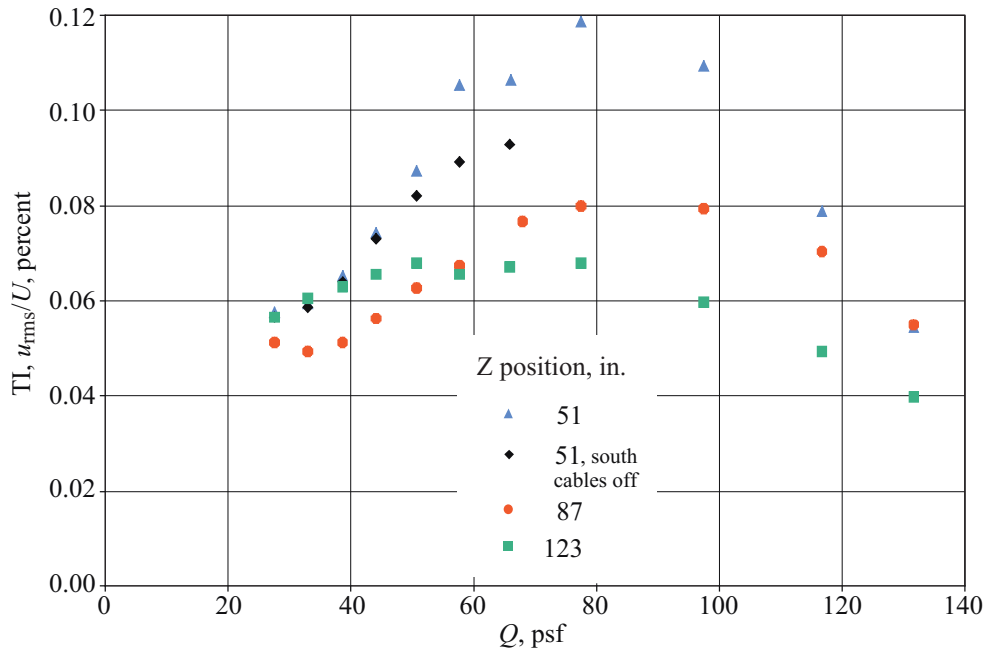


(c) Center of back bay ($X = 40$ ft, $Z = 123$ in.), BLRS on.

Figure 21. Concluded.



(a) BLRS off, $X = 7.87$ ft (beginning of front bay).



(b) BLRS on, $X = 7.87$ ft (beginning of front bay).

Figure 22. Turbulence intensity vertical position effect.

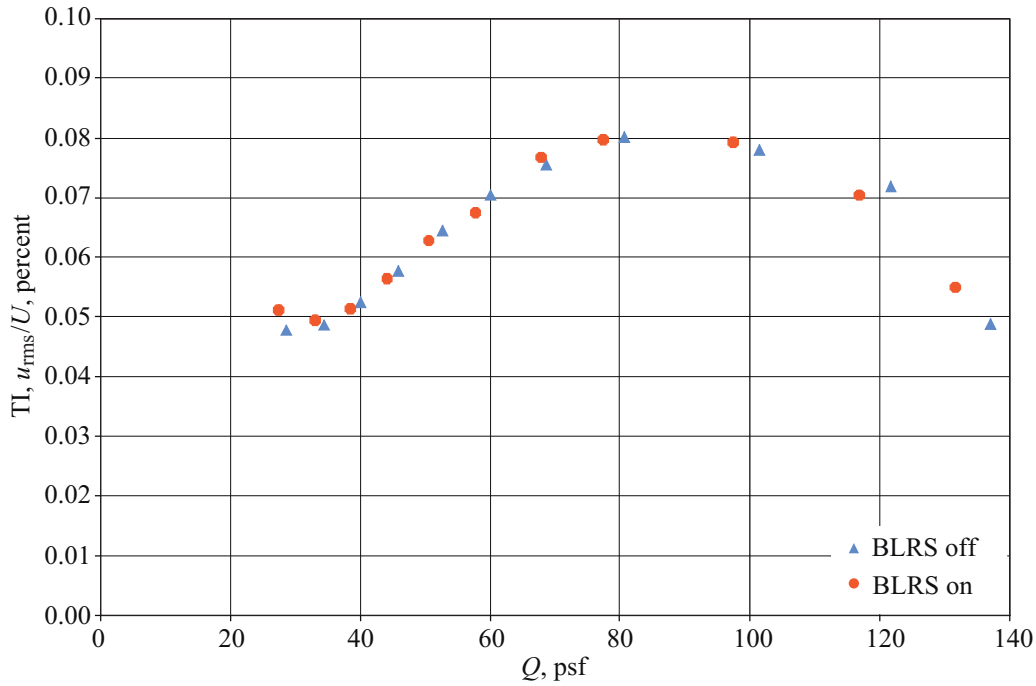


Figure 23. Turbulence intensity, beginning of front bay ($X = 7.87$ ft, $Z = 87$ in.).

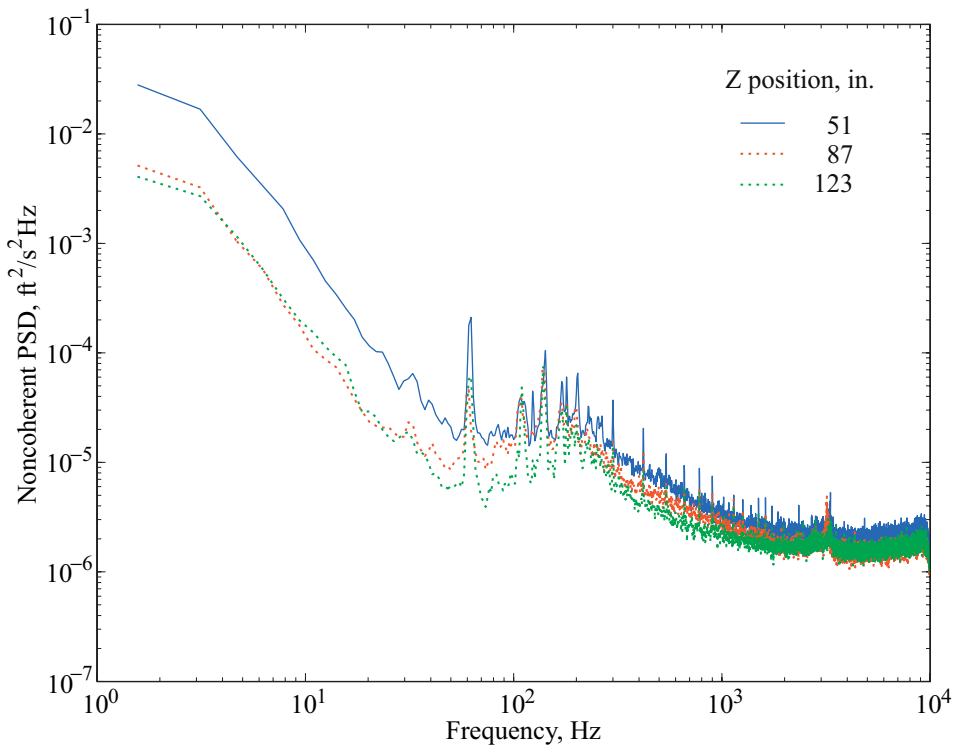
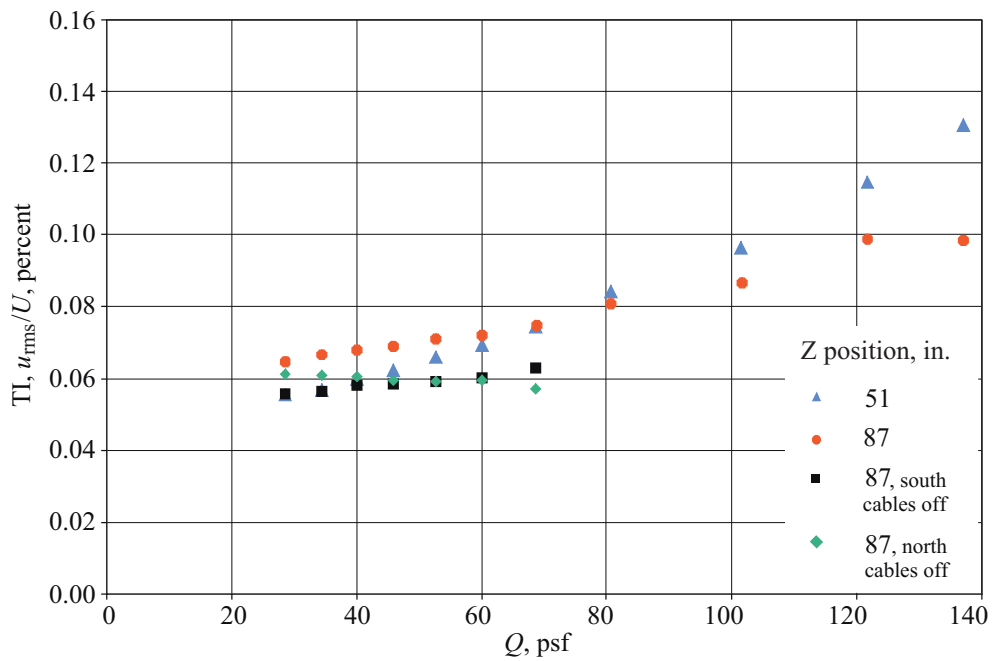
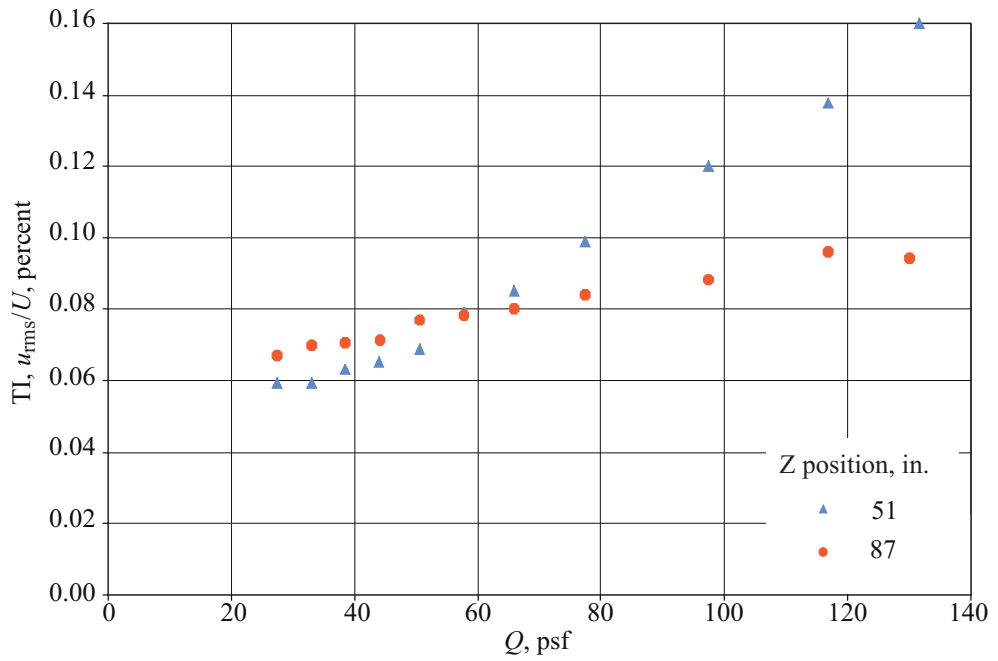


Figure 24. Langley 14- by 22-Foot Subsonic Tunnel, PSD beginning of front bay ($X = 7.87$ ft), BLRS on, $Q = 77$ psf.



(a) BLRS off, $X = 17.75$ ft (center of front bay).



(b) BLRS on, $X = 17.75$ ft (center of front bay).

Figure 25. Turbulence intensity, vertical position effect.

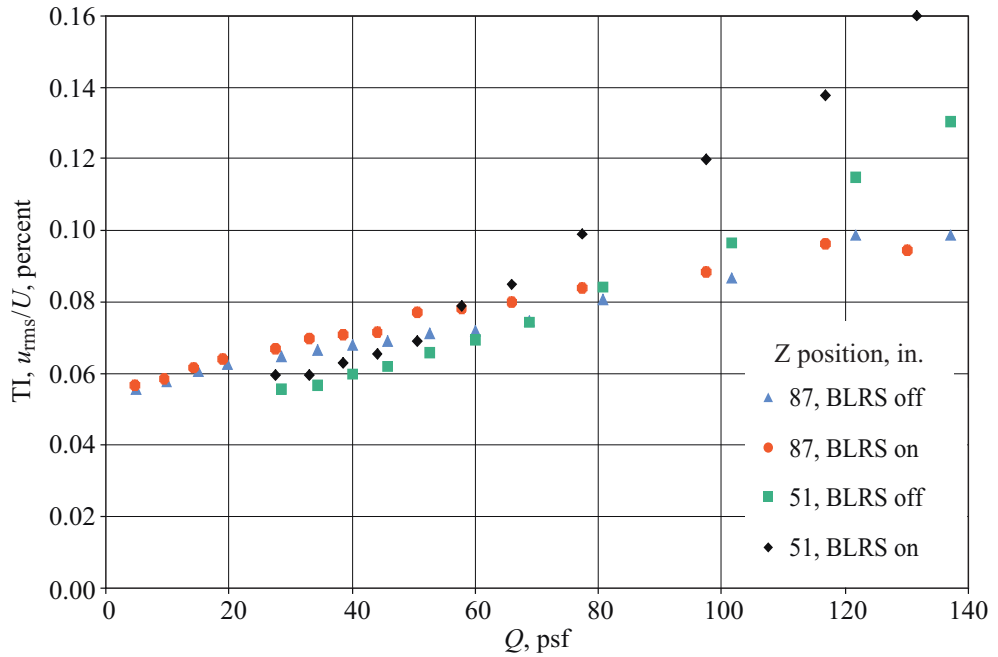


Figure 26. Turbulence intensity, center of front bay ($X = 17.75$ ft).

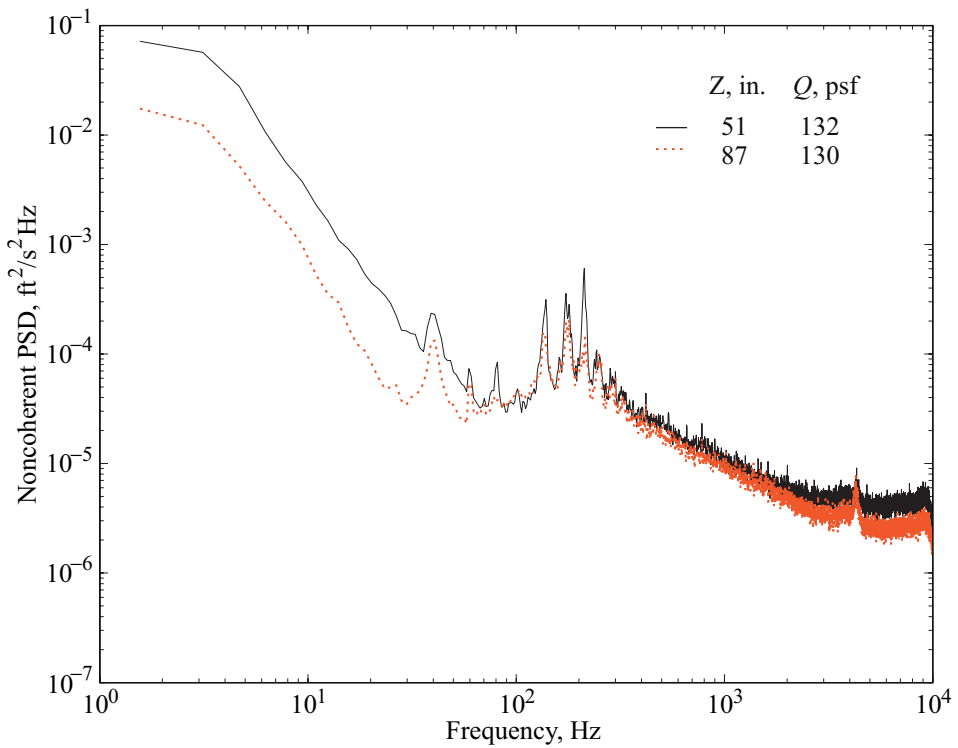
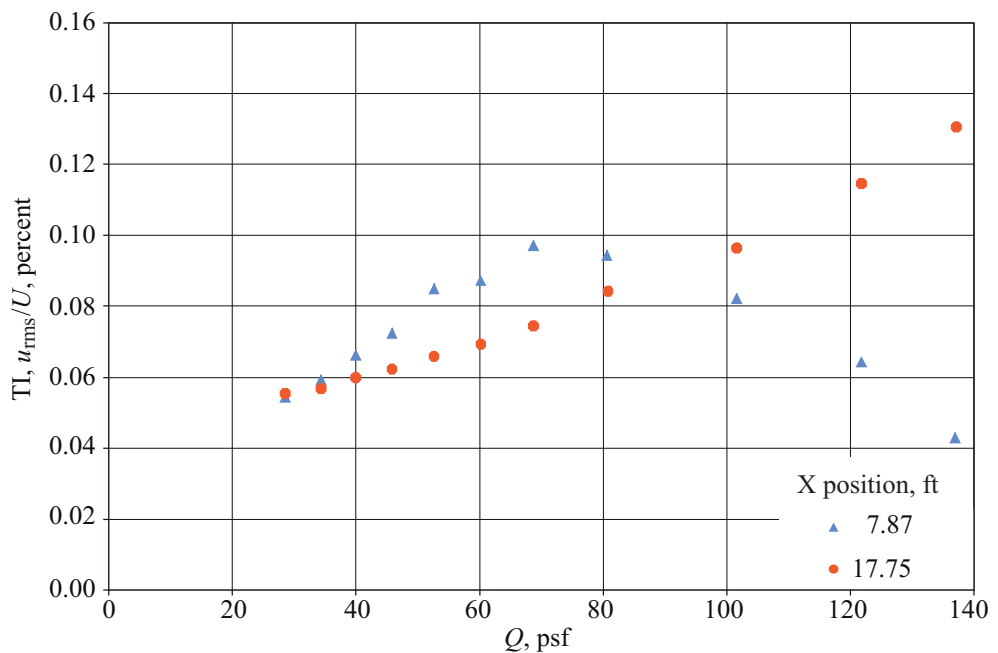
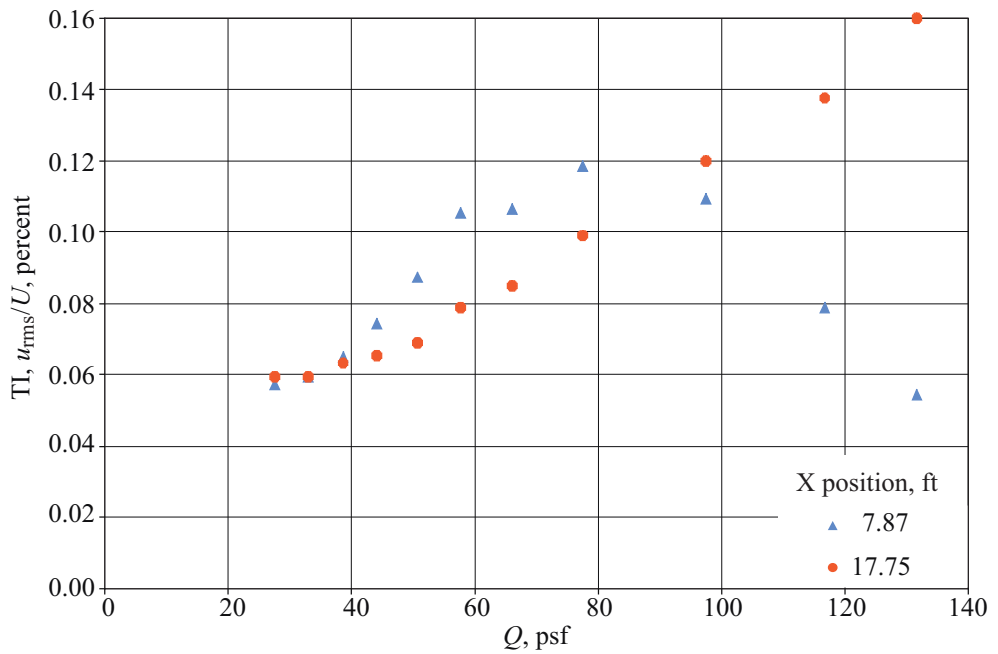


Figure 27. Langley 14- by 22-Foot Subsonic Tunnel PSD, center of front bay ($X = 17.75$ ft), BLRS on.

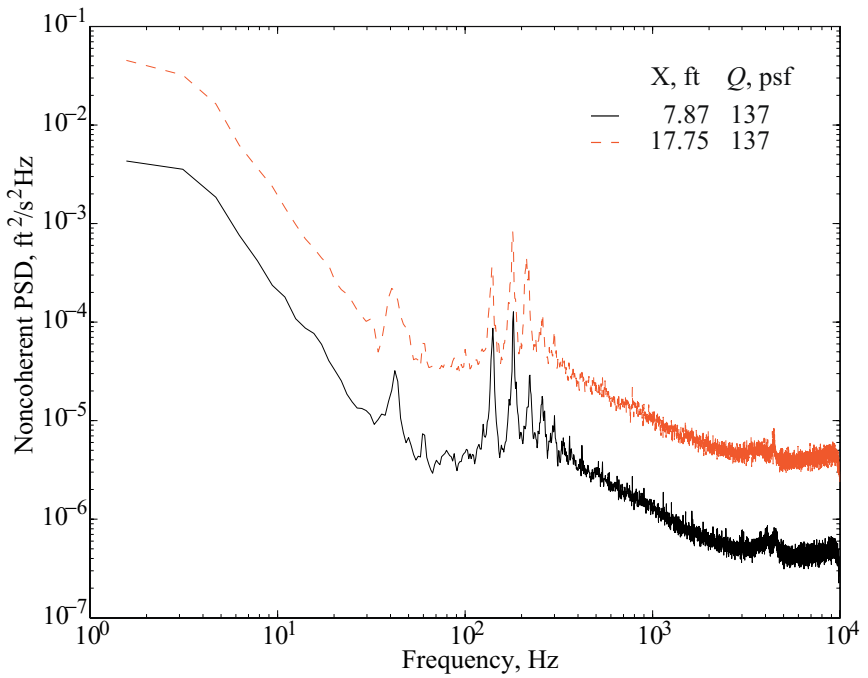


(a) BLRS off, $Z = 51$ in.

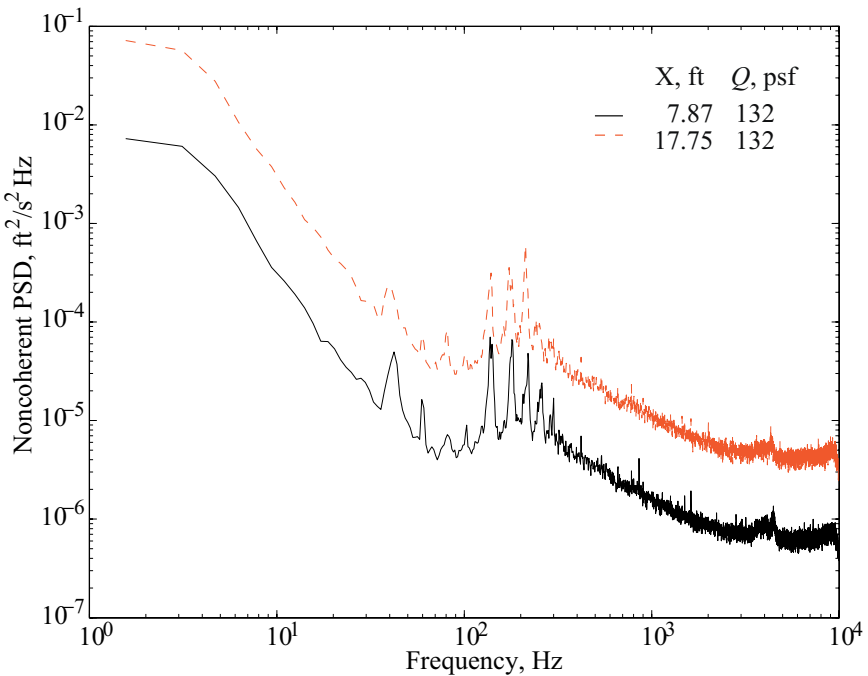


(b) BLRS on, $Z = 51$ in.

Figure 28. Turbulence intensity, longitudinal position effect.

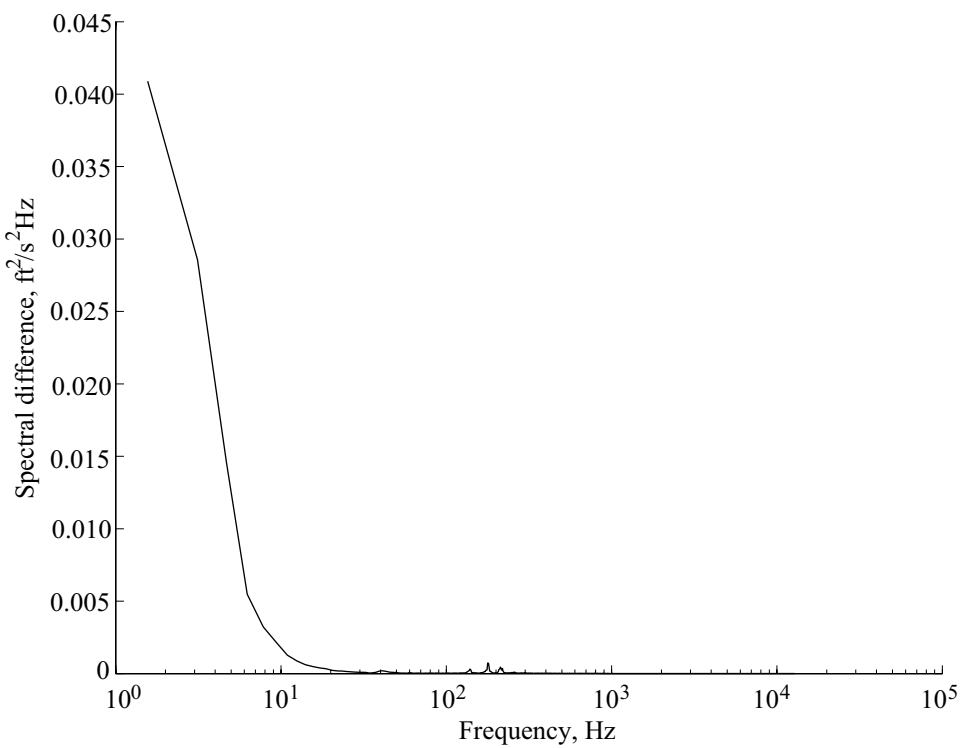


(a) BLRS off.



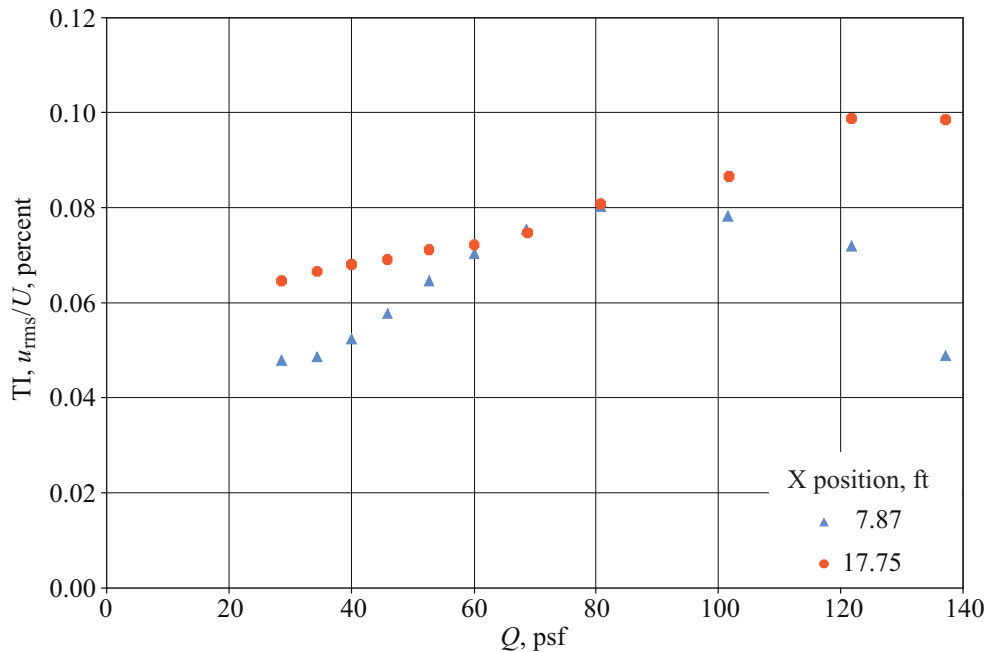
(b) BLRS on.

Figure 29. Langley 14- by 22-Foot Subsonic Tunnel, PSD probe height 51 in.

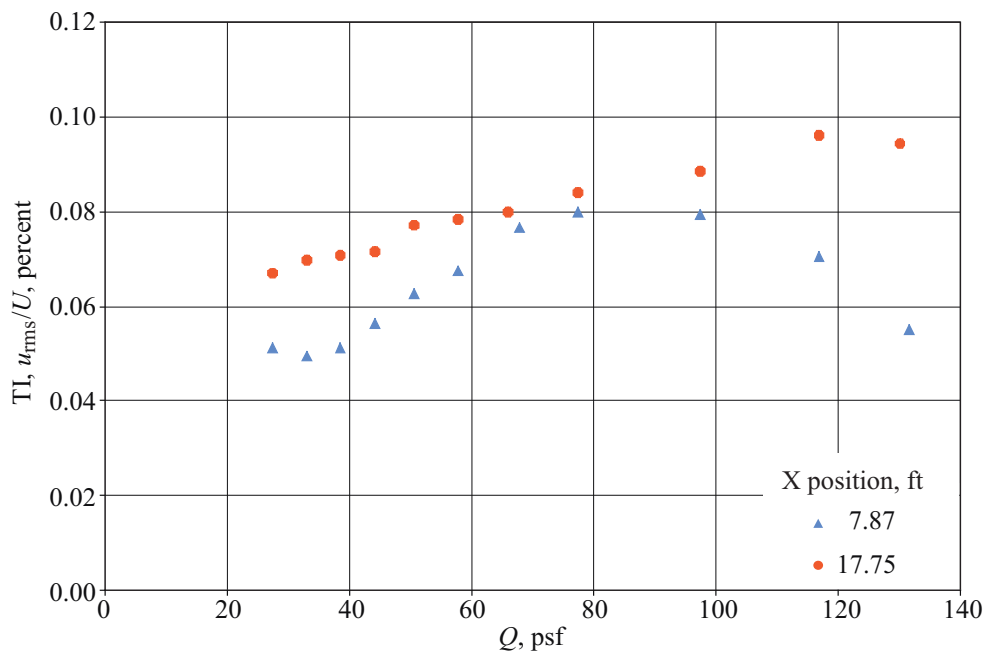


(c) Difference in spectra from figure 29(a), $Q = 137$ psf, BLRS off.

Figure 29. Concluded.

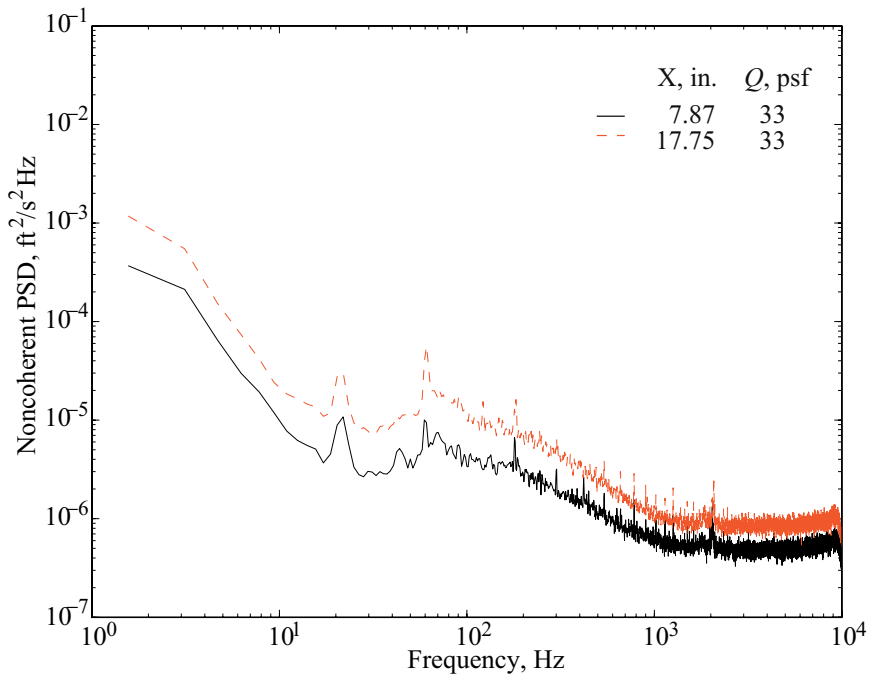


(a) BLRS off, $Z = 87$ in.

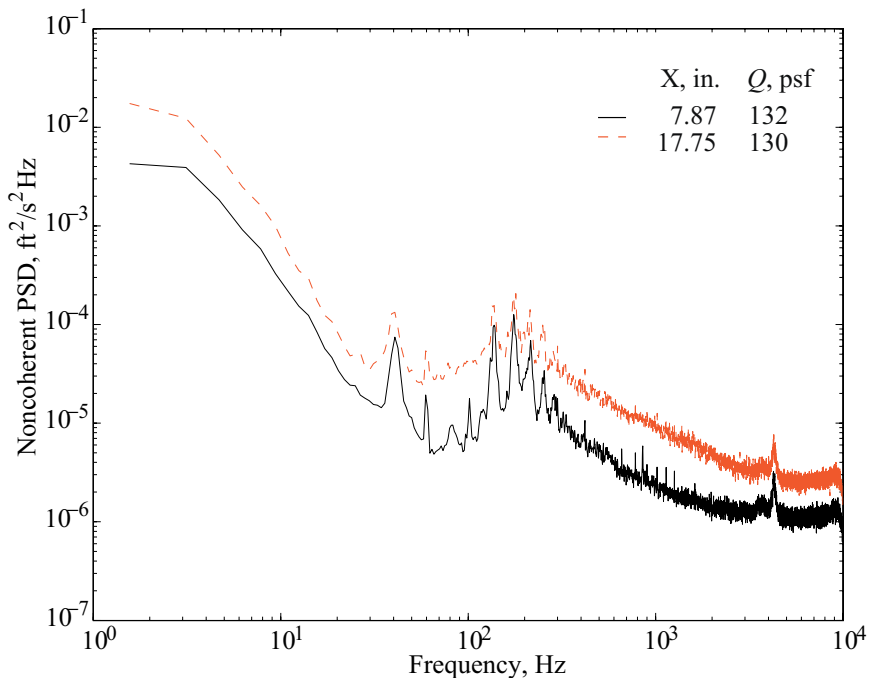


(b) BLRS on, $Z = 87$ in.

Figure 30. Turbulence intensity, longitudinal position effect.

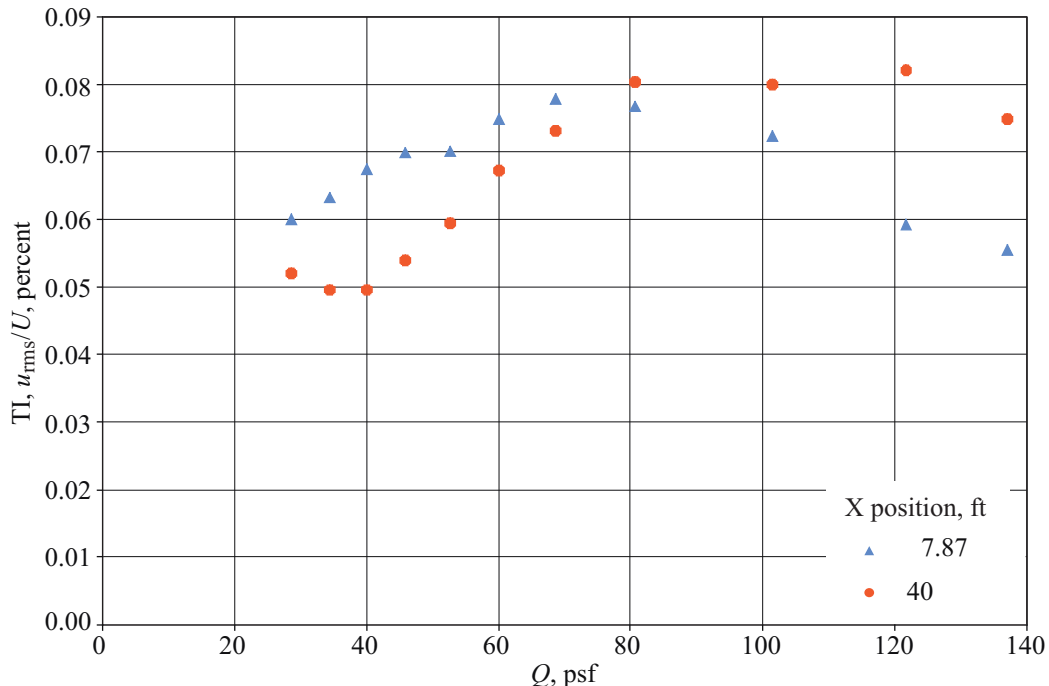


(a) BLRS on, $Q = 33$.

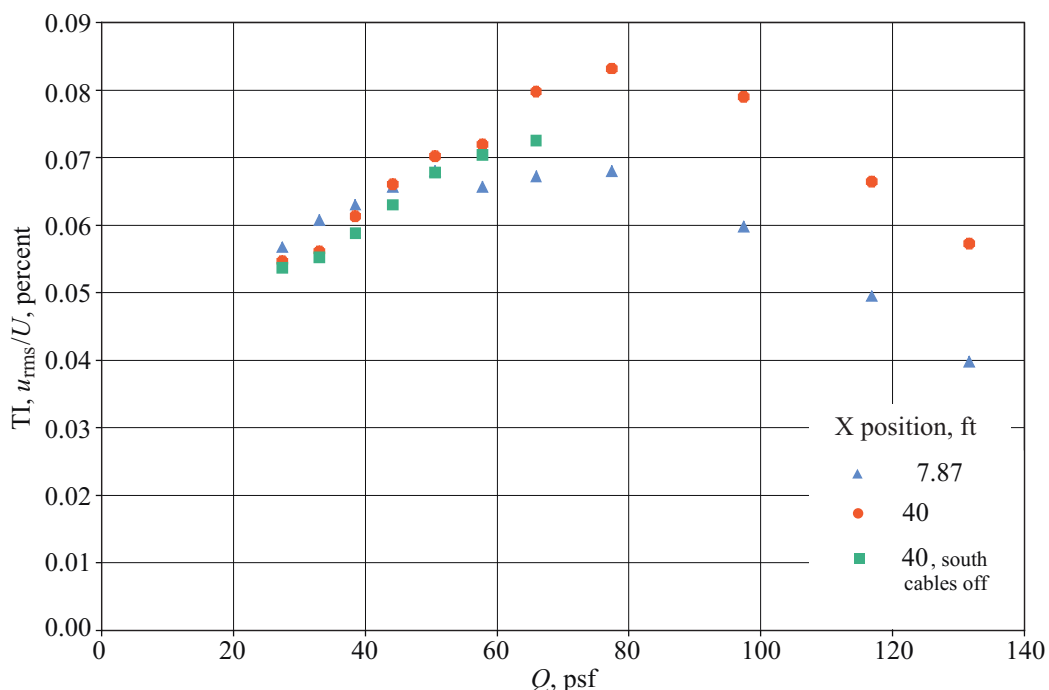


(b) BLRS on, $Q \approx 130$.

Figure 31. Langley 14- by 22-Foot Subsonic Tunnel, PSD probe height 87 in.

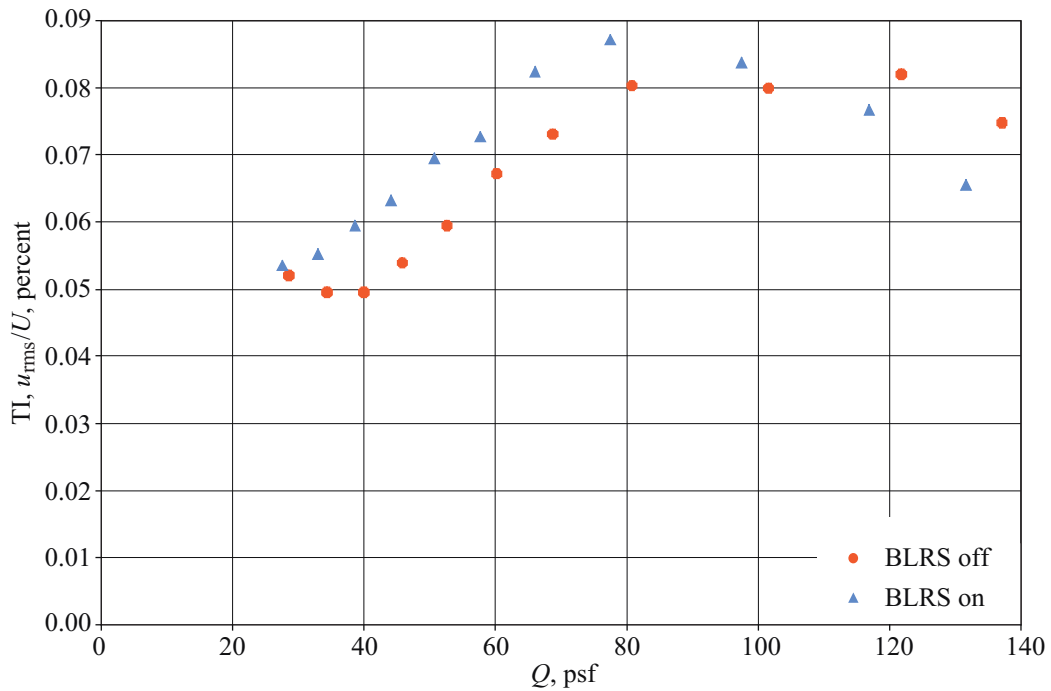


(a) BLRS off, $Z = 123$ in.



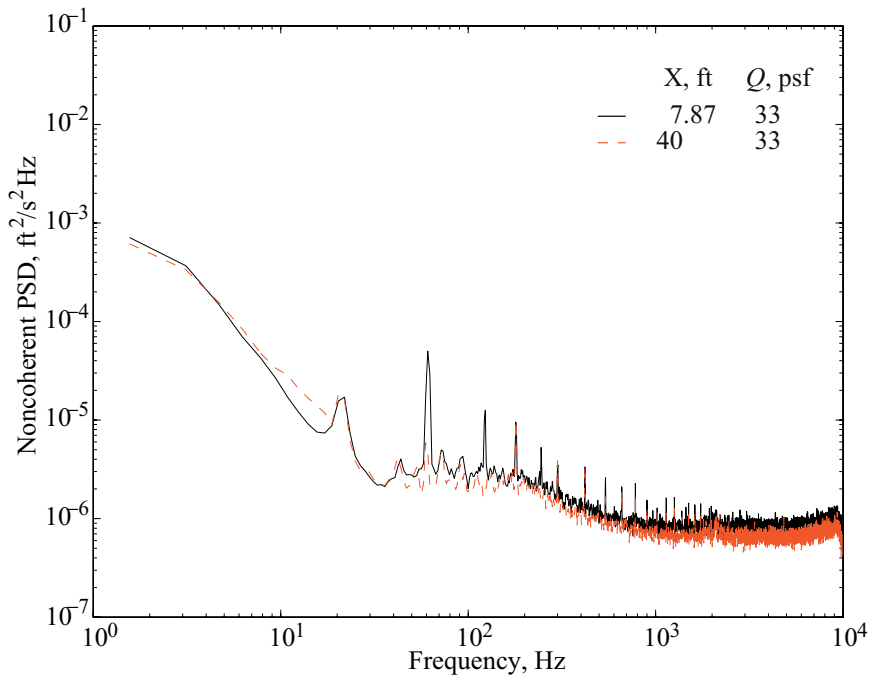
(b) BLRS on, $Z = 123$ in.

Figure 32. Turbulence intensity, longitudinal position effect.

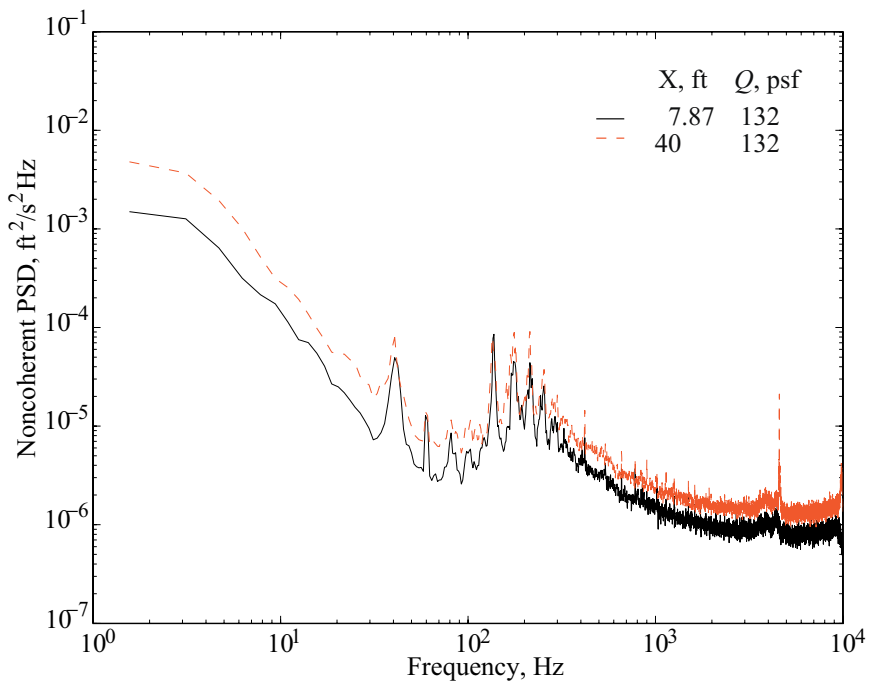


(c) $X = 40$ ft, $Z = 123$ in.

Figure 32. Concluded.



(a) BLRS on, $Q = 33$.



(b) BLRS on, $Q = 132$.

Figure 33. Langley 14- by 22-Foot Subsonic Tunnel, PSD probe height 123 in.

Appendix

Estimation of Experimental Uncertainties

Experimental uncertainties were estimated for mean velocity, U , root-mean-square (rms) fluctuating velocity, and turbulence intensity (TI). The estimation of experimental uncertainties was carried out using techniques similar to those explained in Coleman and Steele (ref. 14).

The process of data acquisition and data reduction was defined first. Then elemental uncertainties in measured quantities were estimated for the various steps in each process and distinguished as either bias (systematic or fixed) uncertainties or precision (random) uncertainties. If there was a calculation involving elemental quantities (e.g., static pressure used to calculate velocity), the uncertainties in these quantities were propagated through data processing equations to arrive at an uncertainty in the calculated quantity. The bias and precision errors (indices) were each summed separately in a root-sum-square (rss) manner and then combined into a total uncertainty. This final uncertainty assumes a 95-percent confidence level, which requires that the precision index, P , be multiplied by a factor of 2 (statistical t distribution value) before being combined in an rss manner with the bias error, B , as follows:

$$U_{\text{rss}} = \left[B^2 + (2P)^2 \right]^{1/2} \quad (\text{A1})$$

In deriving the elemental uncertainties, manufacturer's specifications were used. As is well known, such specifications vary widely in useful content and descriptiveness (or lack thereof). A best effort was made in interpreting and using these specifications.

Propagation of uncertainties in measured quantities, $x_1, x_2, x_3, \dots, x_N$, through data processing equations, was carried out using the equation

$$U_r = \left[\left(\frac{\partial r}{\partial x_1} U_{x_1} \right)^2 + \left(\frac{\partial r}{\partial x_2} U_{x_2} \right)^2 + \dots + \left(\frac{\partial r}{\partial x_N} U_{x_N} \right)^2 \right]^{1/2} \quad (\text{A2})$$

where U_r is the uncertainty in the calculated result r , and U_{x_i} are the uncertainties in the measured variables. This form of the equation was used for the bias and precision errors separately before they were combined into a final uncertainty.

Measurement and Data Reduction Process

The process of making hot-wire measurements was described in the main text of this paper. Figure A1 is a duplication of figure 3, to be used here for description of the derivation of uncertainty estimates in the measured quantities.

The result of a hot-wire measurement is an instantaneous voltage value that is converted into a fluctuating velocity. These velocity fluctuations are used to calculate TI. As shown in the figure, the hot-wire signal passes from the probe to an anemometer unit, from which the total instantaneous analog voltage is derived. The voltage signal is output and split, then sent to a filter unit. The filter unit takes the two voltage signals and low-pass filters, one of them to form the direct current (DC) (mean) signal and band-pass filters, the other signal to form the alternating current (AC) (fluctuating) signal. Each signal is sent to the digitizer (analog-to-digital (A/D) converter), where the signals are digitized separately and sent to the data acquisition computer.

In the lower part of the figure, a pitot-static (PS) probe, for measuring total and static pressure, is shown. Also shown is a shielded thermocouple probe for measuring total temperature. These two probes were used to determine local velocity at the hot-wire station. The data reduction equations for determining velocity from Mach number, M , and the measured quantities, P_t , P_s , and T , are

$$M = \left\{ 5 \left[\left(\frac{P_t}{P_s} \right)^{1/3.5} - 1 \right] \right\}^{1/2} \quad (A3)$$

$$U = 49.02 T^{1/2} M \quad (A4)$$

The measured quantities of temperature and pressure were sent through the facility data acquisition system (DAS) and acquired by the data acquisition computer via an ethernet connection.

Once the voltages, temperatures, and pressures were acquired, the hot-wire calibration process was initiated. In this process, the DC voltages and the corresponding mean velocities were fit to a fourth-order polynomial curve. Temperature corrections were made to the voltages to account for the effect of ambient temperature drift (yielding a ± 0.05 -percent error as opposed to ± 2 percent, uncorrected), providing a corrected calibration curve. The software that computed the five fit coefficients calculated the mean squared error of the fit. The square root of this error was the rms error of the fit, which was used as the precision error for the fit process.

The process for determination of TI continued with the calculation of the power spectral density (PSD) of the velocity fluctuations. First, the total instantaneous velocities were calculated by applying the calibration equation to the total instantaneous voltages, the sum of DC and AC voltages. Then, the velocity fluctuations, u'_i , were calculated by subtracting the mean velocity from the total instantaneous velocity values. The PSD was then performed on the u'_i values, yielding a power spectrum with ordinate units of $(\text{ft/s})^2/\text{Hz}$ versus frequency.

As mentioned in the main text of this paper, noise reduction was performed by using a noise-reduction hot-wire. Coherence between the hot-wire and the noise-reduction hot-wire signals was calculated and used to produce a noncorrelated spectrum. This spectrum was then integrated across the frequency band of interest (1.56 to 10000 Hz), yielding a mean square value of the velocity fluctuations. The square root of this quantity yielded the rms velocity fluctuation, u_{rms} . The turbulence intensity was then calculated as u_{rms} divided by the local mean velocity, U .

Uncertainties in Measured Quantities

The effect of uncertainties in measured quantities on mean velocity for elements of the measurement and data reduction process is shown in table A1.

Table A1. Uncertainties in U Due to Uncertainties in Measured Quantities

Errors	Thermocouple, ref. junction and pressures	Anemometer	Filter	Digitizer	Calibration fit
Bias	5.18*	4.20	9.22	0.284	**
Precision	0.00945	**	**	**	3.10

*All values in units of ft/s.

**Negligible or not applicable.

When “nominal” (nom) conditions are referenced, the following wind tunnel conditions were applied: $M = 0.2$, $U = 225$ ft/s, anemometer signal DC voltage = 2.882 V.

Thermocouples

The thermocouple temperature measurement system consisted of the shielded thermocouple probe (j-type) and the ice point reference junction unit. The errors for this system were assumed to be bias errors and were determined as follows:

Thermocouple	± 4.0 °F
Ice point	± 0.04 °F
Total bias (rss)	± 4.0 °F ($\Delta T/T = \pm 0.04$ for $T_{\text{nom}} = 100$ °F)

Pitot-Static Pressures

One PS pressure system used transducers that measured the absolute total pressure and the differential pressure, from which the static pressure was calculated by subtracting it from the total pressure. This system was used for the hot-wire probes mounted on the stand in the back of the test section, and in the north wall boundary layer rake (for the boundary layer removal system, or BLRS, suction surface replacement study only). The bias errors were calculated using the manufacturer’s accuracy specification. They were

Static pressure	± 0.0039 psi ($\Delta P_s/P_s = \pm 0.00027$ nominal)
Total pressure	± 0.0039 psi ($\Delta P_t/P_t = \pm 0.00026$ nominal)

Precision errors were negligible ($\approx 10^{-6}$ psi).

The electronically scanned pressure (ESP) system was used to sense pressures in the PS probes mounted on the survey rake in the test section and in the wall boundary layer rakes. Their total uncertainty was quoted as ± 0.05 percent of full scale (FS). Because the transducers were 1 psi differential modules, the uncertainties in the pressure measurements made with these modules (which also had atmospheric pressure added and accounted for) were

Static and total pressure	$\Delta P_t = \Delta P_s = \pm 0.0064$ psi ($\Delta P/P = \pm 0.00044$)
---------------------------	--

Anemometer

The anemometer system was determined to have three sources of bias error and one precision error source. The precision error and one of the bias errors that were attributed to this system were actually due to the digital multimeter (DMM) used to set the resistance of the external arm in the anemometer bridge circuit. The bias errors were

Accuracy of resistance, R , measurement	± 0.25 percent R (± 0.25 percent voltage) ($\Delta U/U = \pm 0.018$ nom)
Temperature drift (corrected)	($\Delta U/U = \pm 0.0020$ nom)
DMM bias	± 0.004 Ω ($\Delta U/U = \pm 0.0045$ nom)

Combined in a root-sum-square (rss) manner, these biases gave a total bias error of ± 4.20 ft/s. The precision error was determined to be about 10^{-7} V ($\Delta U = \pm 0.0004$ ft/s) and therefore negligible.

Filter System

The major source of error for the filter system was determined to be the amplitude accuracy of ± 0.05 dB due to passband ripple, which was assumed to be all bias error. This translated to an error or uncertainty in voltage, $\Delta E/E$, of ± 0.57 percent. Using nominal tunnel conditions, this implies a bias error in velocity of $\Delta U = \pm 9.22$ ft/s ($\Delta U/U = \pm 0.041$).

Digitizer (A/D Converter and Signal Conditioning)

The errors due to the digitizer were derived from the amplitude accuracy and amplitude resolution. The digitizer specifications indicated a bias of ± 0.01 -percent FS and 16 bits of resolution, less 2.3 dB over range, for the two bias errors. These specifications translated into a total rss bias error of ± 0.502 mV or ± 0.284 ft/s in velocity.

Precision Error Due to Calibration Curve Fit

As stated earlier, the fourth-order polynomial curve fit of the voltages and velocities yielded five fit coefficients, derived from voltages that were corrected for temperature drift. The calculated mean squared error for a typical curve fit of data taken in the middle of the front bay of the tunnel test section was ± 9.58 (ft/s)². This yielded an rms precision error of ± 3.10 ft/s or $\Delta U/U = \pm 0.0138$ for nominal conditions.

Uncertainties in Calculated Quantities

From equations (A3) and (A4), the uncertainty in calculated local mean velocity was determined as follows.

Because velocity is a function of temperature and Mach number, from equation (A4), the uncertainty in velocity, ΔU , is

$$\Delta U = \left[\left(\frac{\partial U}{\partial T} \Delta T \right)^2 + \left(\frac{\partial U}{\partial M} \Delta M \right)^2 \right]^{1/2} \quad (\text{A5})$$

Mach number is a function of total and static pressures, equation (A3). Therefore, the uncertainty in Mach number, ΔM , is

$$\Delta M = \left[\left(\frac{\partial M}{\partial P_t} \Delta P_t \right)^2 + \left(\frac{\partial M}{\partial P_s} \Delta P_s \right)^2 \right]^{1/2} \quad (\text{A6})$$

The uncertainties in temperature, total pressure, and static pressure in equations (A5) and (A6) have been determined. The derivatives are derived from equations (A3) and (A4). When ΔM was determined in equation (A6), it was inserted into equation (A5), from which the uncertainty in mean local velocity, ΔU , was calculated. This uncertainty was the uncertainty in velocity due to temperature and pressure uncertainties.

The bias in U due to these quantities was ± 5.18 ft/s, and the precision was ± 0.00945 ft/s.

Total Uncertainty in Mean Velocity

The total experimental uncertainty in mean velocity was calculated using equation (A1), where B is the total rss combination of the bias errors in table A1 and P is the rss precision error. The rss combination of the bias and precision indices (errors), using the factor of 2 for the precision index (95 percent confidence level), gave a total uncertainty in mean velocity of ± 12.96 ft/s. This represents a ± 5.76 -percent uncertainty at nominal tunnel conditions. This level of uncertainty in mean velocity is typical for hot-wire anemometry using a single, normal hot-wire probe.

Total Uncertainty in rms Fluctuating Velocity

As described above, the process of determining the individual fluctuating velocities, u'_i , is simply a subtraction of the mean velocity from the total instantaneous velocity values. However, determination of the rms velocity fluctuation (u_{rms}) from these values is computationally complicated and not easily subjected to the type of analysis used above for the determination of uncertainties in mean velocity.

A straightforward method was used to estimate uncertainty in the rms fluctuating velocity. Individual values of fluctuating velocities were adjusted ± 5.76 percent (mean velocity uncertainty) and reprocessed to yield adjusted values of the u_{rms} values. This was done with the nominal case and a case at $M = 0.1$ for comparison. Results of the reprocessing were that, for both cases, the uncertainties in u_{rms} were 5.6 percent of the nominal value at the corresponding Mach number. Based on this limited survey, $\Delta u_{\text{rms}}/u_{\text{rms}} = \pm 0.056$ was used as the uncertainty due to the previously determined factors. An additional consideration, end conduction effects due to heat transfer to the prongs, has been assessed as important by Perry, Smits, and Chong in reference 15. They stated that an additional uncertainty error of ± 10 percent has been observed in mean-square energy due to changes in frequency response, which translates into ± 5 percent in rms turbulence levels. This, then, is added to the uncertainty, in an rss manner, yielding a total uncertainty in u_{rms} of $\Delta u_{\text{rms}}/u_{\text{rms}} = \pm 0.075$.

Total Uncertainty in Turbulence Intensity

Turbulence intensity is defined as $\text{TI} = u_{\text{rms}}/U$. It is usually multiplied by 100 to indicate u_{rms} as a percent of the local mean velocity. Because there are uncertainties in U as well as u_{rms} , an equation for the uncertainty in TI can be derived as

$$\Delta \text{TI}/\text{TI} = \left[\left(\frac{\Delta u_{\text{rms}}}{u_{\text{rms}}} \right)^2 + \left(\frac{\Delta U}{U} \right)^2 \right]^{1/2} \quad (\text{A7})$$

Inserting the uncertainty values calculated above, the uncertainty in TI was estimated to be ± 0.095 or ± 9.5 percent.

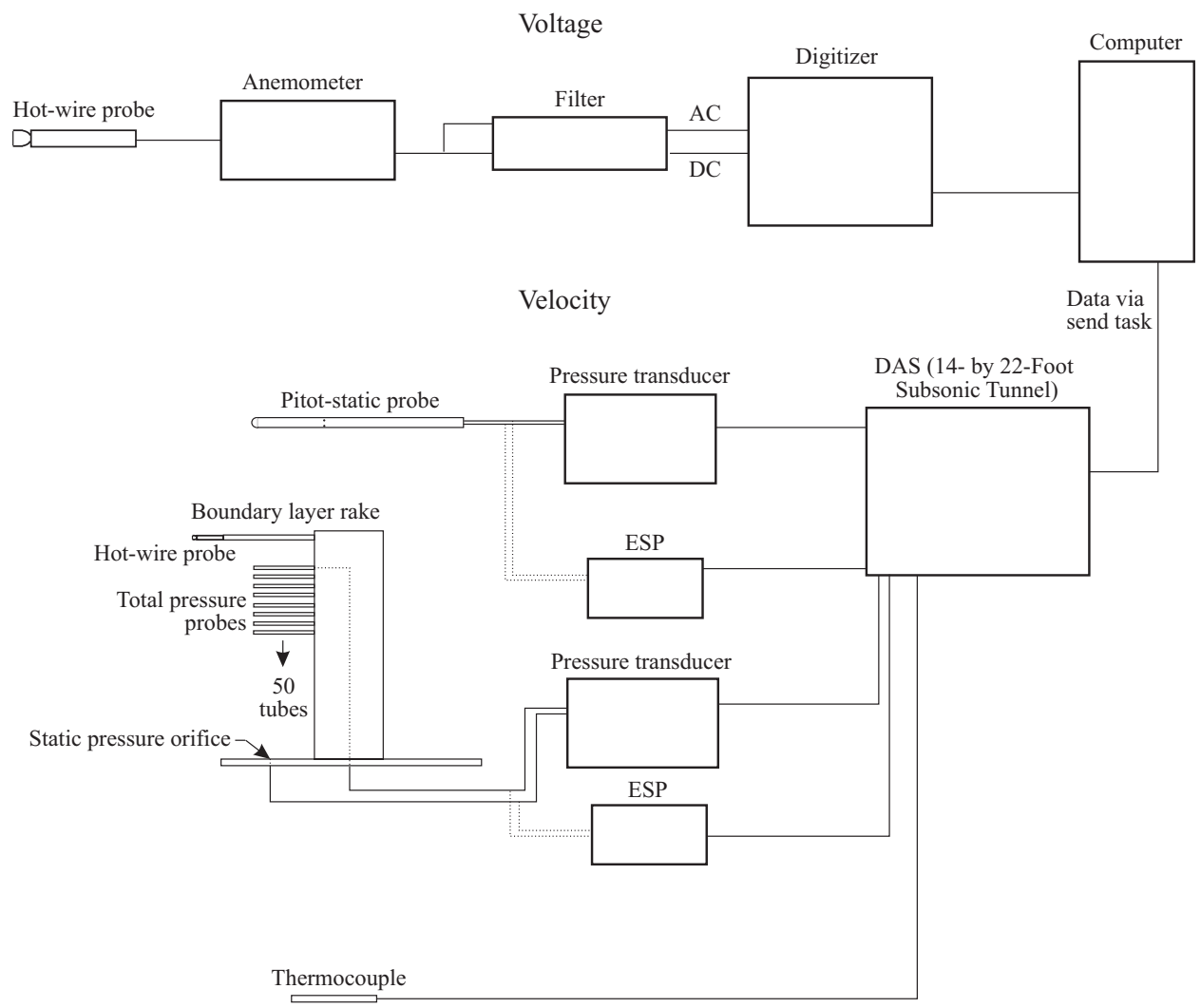


Figure A1. Experimental instrumentation.

References

1. White, Frank M.: *Viscous Fluid Flow*. McGraw-Hill, Inc., 1991.
2. Flow Quality Requirements for Laminar Flow Testing: Phase 2A Deliverable, Item No. 1. NAS3-27330, Aug. 1995.
3. Reshotko, E.; Saric, W. S.; and Nagib, H. M.: Flow Quality Issues for Large Wind Tunnels. AIAA-97-0225, Jan. 1997.
4. Freymuth, Peter: History of Thermal Anemometry. In *Handbook of Fluids in Motion* (eds. N. P. Cheremisinoff and R. Gupta). Ann Arbor Science Publishers, 1983, pp. 79–91.
5. Perry, A. E.: *Hot-Wire Anemometry*. Oxford University Press, 1982.
6. Bruun, H. H.: *Hot-Wire Anemometry*. Oxford University Press, 1995.
7. Gentry, Garl L.; Quinto, P. Frank; Gatlin, Gregory G.; and Applin, Zachary T.: *The Langley 14- by 22-Foot Subsonic Tunnel: Description, Flow Characteristics, and Guide for Users*. NASA TP-3008, 1990.
8. Dantec Dynamics: Improved Temperature Correction in Streamware. Publication No. TN049909.
9. Saric, W. S.; Takagi, S.; and Mousseux, M.: The ASU Unsteady Wind Tunnel and Fundamental Requirements for Freestream Turbulence Measurements. AIAA-88-0053, Jan. 1988.
10. Bendat, Julius S.; and Piersol, Allan G.: *Engineering Applications of Correlation and Spectral Analysis*. John Wiley & Sons, 1993.
11. Wlezien, R. W.; Spencer, S. A.; and Grubb, J. P.: Comparison of Flow Quality in Subsonic Pressure Tunnels. AIAA-94-2503, June 1994.
12. Harris, Julius E.; and Blanchard, Doris K.: *Computer Program for Solving Laminar, Transitional, or Turbulent Compressible Boundary-Layer Equations for Two-Dimensional and Axisymmetric Flow*. NASA TM-83207, 1982.
13. Michel, U.; and Froebel, E.: Flow Unsteadiness in Three Low-Speed Wind Tunnels. In: Data Accuracy and Quality: Requirements and Capabilities in Wind Tunnel Testing. AGARD-CP-429, 1989.
14. Coleman, Hugh W.; and Steele, W. Glenn, Jr.: *Experimentation and Uncertainty Analysis for Engineers*. John Wiley & Sons, Inc., 1989.
15. Perry, A. E.; Smits, A. J.; and Chong, M. S.: The Effects of Certain Low Frequency Phenomena on the Calibration of Hot Wires. *J. Fluid Mech.*, vol. 90, pt. 3, 1979, pp. 415–431.

REPORT DOCUMENTATION PAGE				Form Approved OMB No. 0704-0188	
<p>The public reporting burden for this collection of information is estimated to average 1 hour per response, including the time for reviewing instructions, searching existing data sources, gathering and maintaining the data needed, and completing and reviewing the collection of information. Send comments regarding this burden estimate or any other aspect of this collection of information, including suggestions for reducing this burden, to Department of Defense, Washington Headquarters Services, Directorate for Information Operations and Reports (0704-0188), 1215 Jefferson Davis Highway, Suite 1204, Arlington, VA 22202-4302. Respondents should be aware that notwithstanding any other provision of law, no person shall be subject to any penalty for failing to comply with a collection of information if it does not display a currently valid OMB control number.</p> <p>PLEASE DO NOT RETURN YOUR FORM TO THE ABOVE ADDRESS.</p>					
1. REPORT DATE (DD-MM-YYYY)	2. REPORT TYPE			3. DATES COVERED (From - To)	
01-08-2004	Technical Publication				
4. TITLE AND SUBTITLE			5a. CONTRACT NUMBER 5b. GRANT NUMBER 5c. PROGRAM ELEMENT NUMBER		
Free-Stream Turbulence Intensity in the Langley 14- by 22-Foot Subsonic Tunnel			5d. PROJECT NUMBER 5e. TASK NUMBER 5f. WORK UNIT NUMBER		
6. AUTHOR(S)			5d. PROJECT NUMBER 5e. TASK NUMBER 5f. WORK UNIT NUMBER 762-20-11-80		
7. PERFORMING ORGANIZATION NAME(S) AND ADDRESS(ES)			8. PERFORMING ORGANIZATION REPORT NUMBER NASA L-18336		
NASA Langley Research Center Hampton, VA 23681-2199					
9. SPONSORING/MONITORING AGENCY NAME(S) AND ADDRESS(ES)			10. SPONSOR/MONITOR'S ACRONYM(S) NASA		
National Aeronautics and Space Administration Washington, DC 20546-0001			11. SPONSOR/MONITOR'S REPORT NUMBER(S) NASA/TP-2004-213247		
12. DISTRIBUTION/AVAILABILITY STATEMENT					
Unclassified - Unlimited Subject Category 09 Availability: NASA CASI (301) 621-0390 Distribution: Standard					
13. SUPPLEMENTARY NOTES Neuhart and McGinley, Langley Research Center. An electronic version can be found at http://techreports.larc.nasa.gov/ltrs/ or http://ntrs.nasa.gov					
14. ABSTRACT					
An investigation was conducted using hot-wire anemometry to determine the turbulence intensity levels in the test section of the NASA Langley 14- by 22-Foot Subsonic Tunnel, in the closed or "walls-down" configuration. This study was one component of the three-dimensional, high-lift flow physics experiment designed to provide code validation data. Turbulence intensities were measured during two stages of the study. In the first stage, the free-stream turbulence levels were measured before and after a change was made to the floor suction surface of the wind tunnel's boundary layer removal system. The results indicated that the new suction surface at the entrance to the test section had little impact on the turbulence intensities. The second stage was an overall flow quality survey of the empty tunnel and it included measurements of the turbulence levels at several vertical and streamwise locations. The results indicated that the turbulence intensity is a function of the tunnel dynamic pressure and the location in the test section. The general shape of the frequency spectrum is fairly consistent throughout the wind tunnel, changing mostly in amplitude and slightly with frequency with change in condition and location.					
15. SUBJECT TERMS					
Turbulence intensity; Wind tunnel turbulence; Free-stream turbulence; Subsonic wind tunnels; Fluid flow; Turbulence; Flow quality					
16. SECURITY CLASSIFICATION OF:		a. REPORT	b. ABSTRACT	c. THIS PAGE	17. LIMITATION OF ABSTRACT
		U	U	U	UU
					18. NUMBER OF PAGES
					65
					19a. NAME OF RESPONSIBLE PERSON STI Help Desk (email: help@sti.nasa.gov)
					19b. TELEPHONE NUMBER (Include area code) (301) 621-0390